The Astronomical Journal, 131:1–23, 2006 January

BINARY QUASARS IN THE SLOAN DIGITAL SKY SURVEY: EVIDENCE FOR EXCESS CLUSTERING ON SMALL SCALES

Joseph F. Hennawi,[1,2,3] Michael A. Strauss,[3] Masamune Oguri,[3,4] Naohisa Inada,[5] Gordon T. Richards,[3] Bartosz Pindor,[6,7] Donald P. Schneider,[8] Robert H. Becker,[9,10] Michael D. Gregg,[9,10] Patrick B. Hall,[11] David E. Johnston,[3] Xiaohui Fan,[12] Scott Burles,[13] David J. Schlegel,[14] James E. Gunn,[3] Robert H. Lupton,[3] Neta A. Bahcall,[3] Robert J. Brunner,[15] and Jon Brinkmann[16]

Received 2005 April 25; accepted 2005 August 3

ABSTRACT

We present a sample of 221 new quasar pairs with proper transverse separations $R_{\rm prop} < 1\ h^{-1}$ Mpc over the redshift range $0.5 < z < 3.0$, discovered from an extensive follow-up campaign to find companions around the Sloan Digital Sky Survey and 2dF QSO Redshift Survey quasars. This sample includes 26 new binary quasars with separations $R_{\rm prop} < 50\ h^{-1}$ kpc ($\theta < 10''$), more than doubling the number of such systems known. We define a statistical sample of binaries selected with homogeneous criteria and compute its selection function, taking into account sources of incompleteness. The first measurement of the quasar correlation function on scales $10\ h^{-1}$ kpc $< R_{\rm prop} < 400\ h^{-1}$ kpc is presented. For $R_{\rm prop} \lesssim 40\ h^{-1}$ kpc, we detect an order of magnitude excess clustering over the expectation from the large-scale ($R_{\rm prop} \gtrsim 3\ h^{-1}$ Mpc) quasar correlation function, extrapolated down as a power law ($\gamma = 1.53$) to the separations probed by our binaries. The excess grows to $\sim$30 at $R_{\rm prop} \sim 10\ h^{-1}$ kpc and provides compelling evidence that the quasar autocorrelation function gets progressively steeper on submegaparsec scales. This small-scale excess can likely be attributed to dissipative interaction events that trigger quasar activity in rich environments. Recent small-scale measurements of galaxy clustering and quasar-galaxy clustering are reviewed and discussed in relation to our measurement of small-scale quasar clustering.

Key words: cosmology: observations — large-scale structure of universe — quasars: general — surveys

Online material: color figures, machine-readable tables

1. INTRODUCTION

A fundamental problem for cosmologists is to understand how quasars are embedded in the galaxy formation hierarchy and to relate them to the gravitational evolution of the structure of the underlying dark matter. In the current paradigm, every massive spheroidal galaxy is thought to have undergone a luminous quasar phase, and quasars at high redshift are the progenitors of the local dormant supermassive black hole population found in the centers of nearly all nearby bulge-dominated galaxies (e.g., Small & Blandford 1992; Yu & Tremaine 2002). This fundamental connection is supported by the tight correlations between the masses of central black holes and the velocity dispersions of their old stellar populations (Magorrian et al. 1998; Ferrarese & Merritt 2000; Gebhardt et al. 2000; Tremaine et al. 2002) and by comparing the number density of black holes in the local universe to the luminosity density produced by quasars at high redshift (Small & Blandford 1992; Yu & Tremaine 2002).

Quasars are likely to reside in massive hosts (Turner 1991), and it has been suggested that they occupy the rarest peaks in the initial Gaussian density fluctuation distribution (Efstathiou & Rees 1988; Cole & Kaiser 1989; Nusser & Silk 1993; Djorgovski et al. 1999, 2003; Djorgovski 1999; Stiavelli et al. 2005). It is also thought that quasar activity is triggered by the frequent mergers that are a generic consequence of bottom-up structure formation models (Bahcall et al. 1997; Carlberg 1990; Haehnelt & Rees 1993; Wyithe & Loeb 2002b). Both of these hypotheses imply that quasars should be highly biased tracers of the dark matter distribution: rare peaks in the density field are intrinsically strongly clustered (Kaiser 1984), and the frequency of mergers is higher in dense environments (Lacey & Cole 1993). Measurements of quasar clustering can thus teach us about the environments of quasars, as well as give clues to the dynamical processes that trigger quasar activity. Furthermore, a comparison of quasar clustering with the quasar luminosity function can be used to constrain the mean quasar lifetime (Haiman & Hui 2001; Martini & Weinberg 2001), as well as the relationship between the masses of central black holes and the circular velocities of their host dark halos (Wyithe & Loeb 2005).

There have been many attempts to measure quasar clustering, beginning with the pioneering work of Osmer (1981). Shaver (1984) first detected quasar clustering using a clever technique to

[1] Hubble Fellow.
[2] Department of Astronomy, University of California at Berkeley, 601 Campbell Hall, Berkeley, CA 94720-3411.
[3] Princeton University Observatory, Peyton Hall, Princeton, NJ 08544.
[4] Department of Physics, University of Tokyo, Hongo 7-3-1, Bunkyo-ku, Tokyo 113-0033, Japan.
[5] Institute of Astronomy, University of Tokyo, 2-21-1 Osawa, Mitaka, Tokyo 181-8588, Japan.
[6] Department of Astronomy, University of Toronto, 60 St. George Street, Toronto, ON M5S 3H8, Canada.
[7] CFHT Legacy Survey Postdoctoral Fellow.
[8] Department of Astronomy and Astrophysics, Pennsylvania State University, 525 Davey Laboratory, University Park, PA 16802.
[9] Department of Physics, University of California at Davis, 1 Shields Avenue, Davis, CA 95616.
[10] Institute of Geophysics and Planetary Physics, Lawrence Livermore National Laboratory, L-413, 7000 East Avenue, Livermore, CA 94550.
[11] Department of Physics and Astronomy, York University, 4700 Keele Street, Toronto, ON M3J 1P3, Canada.
[12] Steward Observatory, University of Arizona, 933 North Cherry Avenue, Tucson, AZ 85721.
[13] Physics Department, Massachusetts Institute of Technology, 77 Massachusetts Avenue, Cambridge, MA 02139.
[14] Lawrence Berkeley National Laboratory, One Cyclotron Road, Mail Stop 50-R232, Berkeley, CA 94720.
[15] Department of Astronomy and National Center for Supercomputer Applications, University of Illinois, 1002 West Green Street, Urbana, IL 61801.
[16] Apache Point Observatory, P.O. Box 59, Sunspot, NM 88349-0059.

measure correlations from inhomogeneous catalogs and discovered that quasars were clustered similarly to galaxies in the local universe, a result later confirmed by Kruszewski (1988). Most recently, Croom et al. (2001, 2005) and Porciani et al. (2004, hereafter PMN04) measured the clustering of quasars in the redshift range $z = 0.3$–2.2 from the ∼15,000 quasars in the 2dF QSO Redshift Survey (2QZ; Croom et al. 2004a). They find good agreement with a power-law correlation function $\xi(r) = (r/r_0)^{-\gamma}$ on scales $r = 1$–$35\ h^{-1}$ Mpc, with correlation length $r_0 \sim 5\ h^{-1}$ Mpc (comoving) and slope $\gamma \sim 1.5$, with only a weak dependence on redshift and luminosity (Croom et al. 2002). This agrees with previous measurements (Iovino & Shaver 1988; Andreani & Cristiani 1992; Mo & Fang 1993; Shanks & Boyle 1994; Croom & Shanks 1996; La Franca et al. 1998) and is similar to the clustering of nearby galaxies.

At redshift $z > 2.5$, quasars are rarer, and thus quasar clustering has been much more difficult to measure. However, the mere existence of a few high-redshift quasar pairs provides circumstantial evidence that quasars may have been much more highly clustered in the past. In the Palomar Transit Grism Survey of Schneider et al. (1994), three quasar pairs with $z \gtrsim 3$ and comoving separations 5–10 h^{-1} Mpc were found in a complete sample of 90 quasars covering 61.5 deg^2. Analysis of clustering in this high-redshift sample by Kundic (1997) and Stephens et al. (1997) detected a statistically significant clustering signal, dominated by the three pairs, which implied a comoving correlation length $r_0 \sim 50\ h^{-1}$ Mpc. This is much larger than the correlation length of present-day galaxies or $z \sim 1.5$ quasars. The only subarcminute high-redshift quasar pair known is a $33''$ pair of quasars at $z = 4.25$ discovered serendipitously by Schneider et al. (2000). Based on the discovery of this one object with a proper transverse separation of 162 h^{-1} kpc, they estimated the correlation length could be as large as $\sim 30\ h^{-1}$ Mpc. Djorgovski et al. (2003) discovered a companion at $z = 5.02$ separated by $196''$ from the high-redshift quasar at $z = 4.96$ discovered by Fan et al. (1999), corresponding to a proper transverse separation of 896 h^{-1} kpc. This is the highest redshift pair of quasars known.

Even in the large quasar sample studied by Croom et al. (2001, 2005) and PMN04, the smallest scale at which the correlation function can be measured is $\sim 1\ h^{-1}$ Mpc. The reason for this is twofold. First, close quasar pairs with angular separations $\lesssim 60''$, corresponding to $\sim 1\ h^{-1}$ Mpc at $z \sim 1.5$, are extremely rare, simply because at small separations, the correlation function does not increase as fast as the volume decreases. Second, because of the finite size of the optical fibers of the Two Degree Field (2dF) multiobject spectrograph, only one quasar in a close pair with separation $<30''$ can be observed. This limitation, referred to as a "fiber collision," is also a problem for the Sloan Digital Sky Survey (SDSS; York et al. 2000), for which this angular scale is $55''$ (Blanton et al. 2003).

A significant motivation for studying small-scale quasar clustering is the existence of a controversial population of quasar pairs discovered in the search for gravitationally lensed quasars (Kochanek et al. 1999; Mortlock et al. 1999). These close pairs have similar optical spectra and small velocity differences, and typically have separations in the range $2'' \lesssim \Delta\theta \lesssim 10''$ characteristic of group- or cluster-scale lenses. However, deep imaging shows no identifiable lenses in the foreground. Although a handful of wide-separation ($\Delta\theta > 3''$) gravitational lenses have been discovered (see, e.g., Inada et al. 2003b; Oguri et al. 2005), the expected number of quasars lensed by groups and clusters is too small to account for all the controversial pairs (Oguri & Keeton 2004; Hennawi et al. 2005). The poster child example is Q2345+007 (Weedman et al. 1982), the famous pair of $z = 2.16$ quasars with $7''.1$ separation, for which a plethora of papers can be found in the literature arguing for (Weedman et al. 1982; Turner et al. 1982; Steidel & Sargent 1991; Bonnet et al. 1993; Fischer et al. 1994; Pello et al. 1996; Small et al. 1997) or against (Phinney & Blandford 1986; Djorgovski 1991; Schneider 1993; Kochanek et al. 1999; Mortlock et al. 1999; Green et al. 2002) the lensing hypothesis.

This population has thus led to much speculation about exotic mass concentrations that could be responsible for the apparent multiple imaging. It has been suggested that the lenses in these systems are "dark" galaxies or galaxy clusters (Subramanian et al. 1987; Duncan 1991; Hawkins et al. 1997; Malhotra et al. 1997; Peng et al. 1999; Koopmans et al. 2000), that they could be lensed by free-floating $\sim 10^{14}\ M_\odot$ black holes (Turner 1991), or that they might be instances of gravitational lensing by cosmic strings (Vilenkin 1984; Paczyński 1986; Hogan & Narayan 1984).

A much more plausible explanation is that these controversial pairs are binaries rather than lenses (Phinney & Blandford 1986; Djorgovski 1991; Schneider 1993; Kochanek et al. 1999; Mortlock et al. 1999) and hence just a manifestation of quasar clustering on small scales. Djorgovski (1991) first pointed out that this interpretation implies a factor of ∼100 more binary quasars over what is naively expected from extrapolating the quasar correlation function power law down to comoving scales $\lesssim 100\ h^{-1}$ kpc, and he proposed that this was due to the enhancement of quasar activity during merger events. Based on two close pairs found in the Large Bright Quasar Survey, Hewett et al. (1998) similarly claimed an excess of ∼100 over the expectation from quasar clustering. Kochanek et al. (1999) compared the optical and radio properties of the controversial quasar pairs and argued that they were all binary quasars, and similarly claimed that the excess binaries could be explained in a merger scenario.

The study of binary quasars and small-scale quasar clustering has been hindered by the small number of known examples and the heterogeneous mix of detection methods. In this paper we conduct a systematic search for binary quasars in the SDSS and 2QZ quasar samples. We present a sample of 221 new binary quasars with proper transverse separations $R_{\rm prop} < 1\ h^{-1}$ Mpc, 24 of which have angular separations $\lesssim 10''$ corresponding to transverse proper separations $R_{\rm prop} \lesssim 50\ h^{-1}$ kpc, more than doubling the number of such systems known. A subsample of pairs selected with well-defined criteria is constructed, and we quantify its selection function. Based on this sample, we present the first measurement of the correlation function of quasars on the small scales $10\ h^{-1}$ kpc $\lesssim R_{\rm prop} \lesssim 1\ h^{-1}$ Mpc. We detect excess small-scale clustering compared to the expectation from an extrapolation of the larger scale two-point correlation function power-law slope.

The outline of this paper is as follows: In § 3 we discuss the color-selection criteria used to find binary quasars, and we describe the follow-up observations required to confirm quasar pair candidates in § 4. Our binary quasar sample is presented in § 5. We show that the number of binary quasars discovered thus far in the SDSS implies an excess of small-scale quasar clustering in § 6, and we compare this result to small-scale galaxy and quasar-galaxy clustering in § 7. We summarize and conclude in § 8. In the Appendix we present tables summarizing the results of all our follow-up observations, as well as a catalog of projected quasar pairs from the SDSS.

Throughout this paper we use the best-fit *Wilkinson Microwave Anisotropy Probe* (only) cosmological model of Spergel et al. (2003), with $\Omega_m = 0.270$, $\Omega_\Lambda = 0.73$, and $h = 0.72$. Because both proper and comoving distances are used, we always indicate the former as $R_{\rm prop}$. It is helpful to remember that in the

chosen cosmology, for a typical quasar redshift of $z = 1.5$, an angular separation of $\Delta\theta = 1''$ corresponds to a proper (comoving) transverse separation of $R_{\rm prop} = 6\ h^{-1}$ kpc ($R = 15\ h^{-1}$ kpc), and a velocity difference of 1000 km s^{-1} at this redshift corresponds to a proper radial redshift space distance of $s_{\rm prop} = 4.4\ h^{-1}$ Mpc (comoving $s = 11\ h^{-1}$ Mpc).

2. QUASAR SAMPLES

In this section we present a variety of techniques used to select quasar pair candidates. First, we describe the quasar catalogs that served as the parent samples for our quasar pair search. Then we introduce a statistic that quantifies the color similarity of two quasars. Finally, we discuss each selection method in detail and describe our follow-up observations.

2.1. *The SDSS Spectroscopic Quasar Sample*

The SDSS uses a dedicated 2.5 m telescope and a large-format CCD camera (Gunn et al. 1998) at the Apache Point Observatory (APO) in New Mexico to obtain images in five broad bands (u, g, r, i, and z, centered at 3551, 4686, 6166, 7480, and 8932 Å, respectively; Fukugita et al. 1996; Stoughton et al. 2002) of high Galactic latitude sky in the northern Galactic cap. The imaging data are processed by the astrometric pipeline (Pier et al. 2003) and photometric pipeline (Lupton et al. 2001) and are photometrically calibrated to a standard star network (Smith et al. 2002; Hogg et al. 2001). Additional details on the SDSS data products can be found in Abazajian et al. (2003, 2004, 2005).

Based on this imaging data, spectroscopic targets chosen by various selection algorithms (i.e., quasars, galaxies, stars, and serendipity) are observed with two double spectrographs producing spectra covering 3800–9200 Å, with a spectral resolution ranging from 1800 to 2100. Details of the spectroscopic observations can be found in York et al. (2000), Castander et al. (2001), and Stoughton et al. (2002). A discussion of quasar target selection can be found in Richards et al. (2002b). The Third Data Release (DR3) quasar catalog contains 46,420 quasars (Schneider et al. 2005). Here we use a larger sample of quasars, as we include nonpublic data: our parent sample includes 67,385 quasars with $z > 0.3$, of which 52,279 lie in the redshift range $0.7 < z < 3.0$. Note also that we have used the Princeton/Massachusetts Institute of Technology spectroscopic reductions,[17] which differ slightly from the official SDSS data release.

Most quasar candidates are selected based on their location in multidimensional SDSS color space. All magnitudes are reddening corrected following the prescription in Schlegel et al. (1998). Objects with colors that place them outside of the stellar locus that do not inhabit specific "exclusion" regions (e.g., places dominated by white dwarfs, A stars, and M star–white dwarf pairs) are identified as primary quasar candidates. An i magnitude limit of 19.1 is imposed for candidates whose colors indicate a probable redshift of less than $\approx$3; high-redshift candidates are accepted if $i < 20.2$. Over 90% of SDSS-selected quasars follow a remarkably tight color-redshift relation in the SDSS color system (Richards et al. 2001a). In addition to the multicolor selection, unresolved objects brighter than $i = 19.1$ that lie within $1\farcs5$ of a FIRST radio source (Becker et al. 1995) are also identified as primary quasar candidates.

Supplementing the primary quasar sample described above are quasars targeted by other SDSS target-selection packages: Galaxy (the SDSS main and extended galaxy samples; Eisenstein et al. 2001; Strauss et al. 2002), X-ray (objects near the position of a *ROSAT* All-Sky Survey source; Anderson et al. 2003), Star (point sources with unusual color), or Serendipity (unusual color or FIRST matches). No attempt at completeness is made for the last three categories; objects selected by these algorithms are observed if a given spectroscopic plate has fibers remaining after all the high-priority classes (galaxies, quasars, and sky and spectrophotometric calibrations) in the field have been assigned fibers (see Blanton et al. 2003). Most of the quasars that fall below the magnitude limits of the quasar survey were selected by the serendipity algorithm.

As we described in § 1, the spectroscopic SDSS selects *against* close pairs of quasars because of fiber collisions. The finite size of optical fibers implies that only one quasar in a pair with separation $<55''$ can receive a fiber. Follow-up spectroscopy is thus required to discover quasar pairs. An exception to this rule exists for a fraction ($\sim$30%) of the area of the spectroscopic survey covered by overlapping plates. For these plates the same area of sky was observed spectroscopically on more than one occasion, so that there is no fiber collision limitation.

2.2. *The SDSS Faint Photometric Quasar Sample*

Richards et al. (2004) have demonstrated that faint ($i \lesssim 21$) photometric samples of quasars can be constructed from the SDSS photometry by separating quasars from stars using knowledge of their relative densities in color space. Each member of this catalog is assigned a probability of being a quasar, a photometric redshift, and a probability that the photometric redshift is correct (see Richards et al. 2004 for details). We searched for (and found) quasar pairs in a photometric sample of 273,287 quasar *candidates*. Note that the faint photometric quasar used here is based on the larger SDSS DR3 area (Abazajian et al. 2005), whereas that published in Richards et al. (2004) covers the smaller SDSS DR1 area (Abazajian et al. 2003).

2.3. *The SDSS + 2QZ Quasar Sample*

The 2QZ is a homogeneous spectroscopic catalog of 44,576 stellar objects with $18.25 \leq b_{\rm J} \leq 20.85$ (Croom et al. 2004a). Of these, 23,338 are quasars spanning the redshift range $0.3 \lesssim z \lesssim 2.9$. Selection of quasar candidates is based on broadband colors ($ub_{\rm J}r$) from automated plate measurements of the United Kingdom Schmidt Telescope photographic plates. Spectroscopic observations were carried out with the 2dF instrument, which is a multiobject spectrograph at the Anglo-Australian Telescope. The 2QZ covers a total area of 721.6 deg^2 arranged in two $75^\circ \times 5^\circ$ strips across the southern Galactic cap (south Galactic pole strip), centered on $\delta = -30^\circ$, and the northern Galactic cap (north Galactic pole [NGP] strip, or equatorial strip), centered at $\delta = 0^\circ$. The NGP overlaps the SDSS footprint, corresponding to roughly half of the 2QZ area.

By combining the SDSS quasar catalog with 2QZ quasars in the NGP that have matching SDSS photometry, we arrive at a combined sample of 75,579 quasars with $z > 0.3$, of which 67,385 are from the SDSS and 8194 from the 2QZ. For the clustering analysis in § 6 we restrict attention to the redshift range $0.7 < z < 3.0$, for which we define a combined SDSS + 2QZ sample of 59,608 quasars, of which 52,279 are from the SDSS and 6879 from the 2QZ.

3. QUASAR PAIR SELECTION

Several different techniques are used to find binary quasars. For small-separation pairs, $\Delta\theta \leq 3''$, characteristic of the majority of gravitational lenses, binary quasars were discovered in

[17] Available at http://spectro.princeton.edu.

the SDSS search for gravitationally lensed quasars (e.g., Oguri et al. 2005). For wider separations, both components are resolved and we can exploit the precise digital photometry of the SDSS to color-select quasar pair candidates. Finally, quasar pairs can be found directly from the spectroscopy; the SDSS contains a fair number of overlapping spectroscopic plates for which fiber collision does not limit the pair separation, and quasar pairs can be found by searching the SDSS + 2QZ quasar catalog over regions where the survey areas overlap.

3.1. *Lens Selection*

For small-separation pairs $\Delta\theta \leq 3''$, the two images are unresolved or marginally resolved, as the SDSS imaging has a median seeing of $1''.4$. Candidates are selected by fitting a multicomponent point-spread function (PSF) model to atlas images of each of the SDSS quasars as described in Pindor et al. (2003) and Inada et al. (2003a). We restricted attention to candidates in the redshift range $0.7 < z < 3.0$. Quasars with $z < 0.7$ are unlikely to be gravitational lenses, and the PSF fitting is complicated by the presence of resolved host galaxy emission. The SDSS is biased against gravitational lenses with $z > 3.0$ because the target selection algorithm for high-z quasars does not target objects classified as extended by the photometric pipeline, and most candidate lenses and binaries appear extended. See the discussion in Pindor et al. (2003) for more details. The number of quasars in this redshift range searched with our lens algorithm was 39,142, which makes up the parent sample of our lens search. This is a subset of the total number (52,279) of SDSS quasars in this range, as the lens algorithm was run on a sample of quasars defined at an earlier date. We refer to objects selected by this algorithm as the "lens" sample.

Follow-up observations are required to confirm that the companion object is indeed a quasar at the same redshift. The limiting magnitude for the companion objects is $i < 21.0$ (here and throughout we always quote reddening-corrected asinh magnitudes; Lupton et al. 1999), as fainter objects are too difficult to observe from the 3.5 m telescope at APO, where most of the follow-up observations were conducted, even in the best conditions (see § 4).

3.2. χ^2 *Color Selection*

Although quasars have a wide range of luminosities, the majority have similar optical/ultraviolet spectral energy distributions. Richards et al. (2001a) demonstrated that most quasars follow a relatively tight color-redshift relation in the SDSS filter system, a property that has been exploited to calculate photometric redshifts of quasars (Richards et al. 2001b; Budavári et al. 2001; Weinstein et al. 2004). It is thus possible to efficiently select pairs of quasars at the same redshift by searching for pairs of objects with similar, quasar-like colors.

To this end, we define a statistic that quantifies the likelihood that two astronomical objects have the same color. Recall that a color $u - g$ is a statement about flux *ratios*, f^u/f^g. Thus, if two objects have the same color, then their fluxes should be proportional. Given the fluxes f_1^m of the first, we can ask whether the fluxes of the second are consistent with the proportionality

$$f_2^m = A f_1^m, \tag{1}$$

where f^m is a five-dimensional vector of fluxes (one for each SDSS band), m designates the filter, and this relationship holds with the same proportionality constant A in all bands.

The maximum likelihood value of the parameter A, given the fluxes of both objects, can be determined by minimizing the χ^2:

$$\chi^2(A) = \sum_{ugriz} \frac{\left(f_2^m - A f_1^m\right)^2}{\left(\sigma_2^m\right)^2 + A^2\left(\sigma_1^m\right)^2}, \tag{2}$$

where we have dropped a term corresponding to the normalization of the likelihood because of its slow variation with the parameter A. The σ^m are the photometric measurement errors but do not include the intrinsic scatter about the mean color–redshift relation (see the discussion below). We thus arrive at the implicit equation for A:

$$A = \frac{\sum_{ugriz} f_2^m f_1^m / \left(\left[\sigma_2^m\right]^2 + A^2\left[\sigma_1^m\right]^2\right)}{\sum_{ugriz} \left[f_2^m\right]^2 / \left(\left[\sigma_2^m\right]^2 + A^2\left[\sigma_1^m\right]^2\right)}, \tag{3}$$

which can be solved in a few iterations. This value is inserted into equation (2), reducing the number of degrees of freedom in χ^2 to 4, i.e., the number of independent colors one could have formed from the five magnitudes.

If the fluxes of the two objects are proportional and if the photometric errors are distributed normally, this statistic follows the χ^2 distribution with 4 degrees of freedom, and the typical value is $\chi^2 \sim 4$. However, the colors of two quasars at the same redshift, although similar, will in general not be exactly proportional. Fluctuations about the median color–redshift relation of quasars (Richards et al. 2001a) will result in an additional source of "dispersion" in our color similarity statistic. This leads to a much broader distribution of χ^2 than expected from Gaussian statistical errors. Figure 1 shows the distribution of χ^2 for the 64,621 unique pair combinations of 359 quasars in the redshift interval $2.4 < z < 2.45$. The median value of this distribution is 33.1, so that a quasar pair survey that aims to achieve 50% completeness in this redshift interval would have to observe all quasar pair candidates with $\chi^2 < 33.1$. Also notice that a long tail in this distribution extends even beyond $\chi^2 \sim 100$ because of outliers from the median color–redshift relation of quasars (Richards et al. 2001a), caused by broad absorption line features (Richards et al. 2003) or reddening (Hopkins et al. 2004).

Our survey for close pairs of quasars thus involves a tradeoff between completeness and efficiency, since tolerating larger values of χ^2 will increase the number of false pair candidates. Our follow-up observations targeted quasar pair candidates with $\chi^2 < 20$. This threshold implies a certain level of completeness for our survey, which varies with redshift, as the dispersion in the color-redshift relation of quasars depends on redshift (Richards et al. 2001a). We quantify this incompleteness by dividing the SDSS quasar sample into redshift bins of $\delta z = 0.043$ and computing the fraction of all the unique combinations of pairs in each bin with $\chi^2 < 20$. Figure 2 shows the completeness of our quasar pair survey as a function of redshift. For the redshift range $0.70 < z < 3.0$, where most of our binary quasars lie, the $\chi^2 < 20$ cut results in ~35% completeness.

Finally, note that the statistic defined by equation (2) uses an isotropic "metric" in color space. This would not be the case had we included the variance of the color-redshift relation $\sigma^m(z)$ in our errors $\sigma^m_{\rm total}$, similar to the procedure used by Richards et al. (2001b) and Weinstein et al. (2004) to determine photometric redshifts of quasars. In retrospect, this would be a more suitable procedure for finding binary quasars. However, we were also

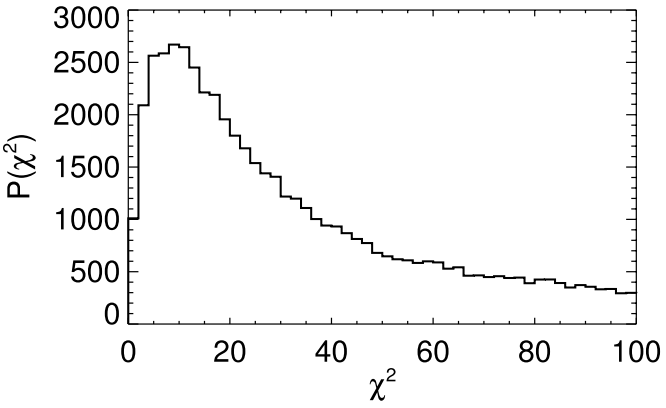

FIG. 1.—Histogram of the χ^2 color similarity statistic (see eq. [2]) values for 64,621 unique pair combinations of 359 quasars in the SDSS sample in the narrow redshift interval $2.4 < z < 2.45$. Although the quasars are all at nearly the same redshift, $z \simeq 2.4$, the dispersion in the color-redshift relation of quasars (Richards et al. 2001a) results in a broad distribution. The median value is 33.1, so that a quasar pair survey that aims to achieve 50% completeness for $z \simeq 2.4$ quasars would have to observe all quasar pair candidates with $\chi^2 < 33.1$.

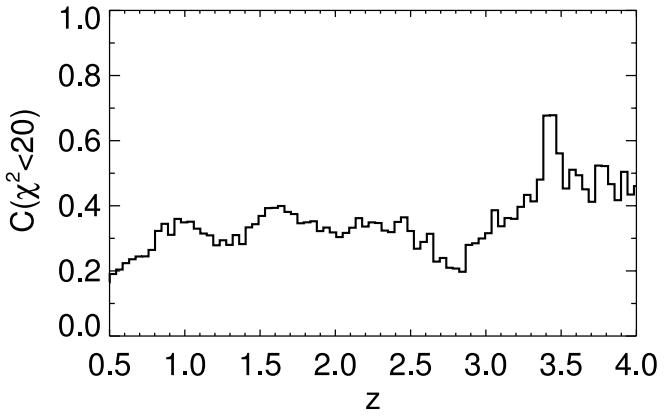

FIG. 2.—Completeness of the χ^2 color similarity statistic (see eq. [2]) as a function of redshift for a quasar pair survey that observes all quasar pair candidates with $\chi^2 < 20$. The dispersion in the color-redshift relation of quasars (Richards et al. 2001a) gives rise to a broad distribution of χ^2 for pairs of quasars at the same redshift (see Fig. 1). As the amount of color dispersion varies with redshift, so does the fraction of quasar pairs recovered for $\chi^2 < 20$. Restricting the observations of pair candidates to those with $\chi^2 < 20$ results in ~35% completeness in the redshift range $0.70 < z < 3.0$.

conducting a search for wide-separation gravitational lenses, and for lenses there is no color-redshift scatter. (After all, it is the same quasar observed twice!)

We applied our color similarity statistic to all objects within the annulus $3'' < \Delta\theta < 60''$ around the 59,608 quasars ($0.7 < z < 3.0$) in the combined SDSS + 2QZ catalog. We refer to the binaries selected by searching around the SDSS + 2QZ quasars as members of our "χ^2" sample. To be considered for follow-up observations, a quasar pair had to meet the following criteria:

$$\chi^2 < 20.0, \quad 0.70 < z < 3.0, \quad i < 21.0, \quad \sigma_i < 0.2. \quad (4)$$

The minimum redshift was imposed because of our desire to find wide-separation gravitational lenses (Inada et al. 2003b; Oguri et al. 2004). The $\sigma_i < 0.2$ requirement gets rid of objects with very large photometric errors due to problems with deblending or very poor image quality. In addition, we required that the companion objects be optically unresolved in the SDSS imaging to avoid contamination from galaxies. Nearly all quasars at $z > 0.70$ should be unresolved in the SDSS imaging, with the exception of very small separation pairs, $<3''$; however, these pair candidates are selected by our algorithm described in § 3.1.

We also used the criteria in equation (4) to search for pair candidates in the catalog of 273,287 faint photometric quasars. We restricted attention to members of the catalog only and did not consider other nearby photometric objects. We refer to binaries discovered in this catalog as our "photometric" sample. The same criteria as in equation (4) were used, but there were no lower or upper limits on redshift since spectroscopic redshifts were not available for this sample.

3.3. *Overlap and Spectroscopic Selection*

As mentioned previously, the SDSS contains a fair number of overlapping spectroscopic plates for which fiber collision does not limit the pair separation. Furthermore, quasar pairs can be found below the fiber collision limits by searching the SDSS + 2QZ quasar catalog over regions where the survey areas overlap. Finally, for separations $\theta \geq 60''$, larger than the SDSS fiber collision scale,[18] quasar pairs can be found in the entire SDSS area. We refer to pairs found in the spectroscopic catalog with $\theta \leq 60''$ as our "overlap" sample, and we refer to those with $\theta > 60''$ as our "spectroscopic" sample. No color similarity criteria were applied to these objects, and the only magnitude or error limits are those imposed by the SDSS target selection (Richards et al. 2002b).

3.4. *Previously Known Binaries*

It is instructive to ask whether previously known binary quasars are selected by our selection techniques. In Table 1 we list the nine previously known binary quasars with $0.7 \lesssim z \lesssim 3.0$ that are in the SDSS footprint, of which seven were recovered. The column labeled "Sample" indicates the sample for which each binary was selected as a candidate. Six of these binaries are listed in the compilation of binary quasars on the CASTLES Web site.[19] The others are SDSS J2336−0107 (Gregg et al. 2002) and SDSS J1120+6711 (Pindor et al. 2006), discovered recently in the SDSS search for gravitational lenses, and 2QZ J1435+0008, the $33''$ pair of quasars discovered in the 2QZ by Miller et al. (2004).

Of the nine binaries listed in the table, all but Q1343+2650, Q1635+267, and 2QZ J1435+0008 had at least one member of the pair in the SDSS spectroscopic sample. Neither member of the pairs Q1343+2650 and 2QZ J1435+0008 was targeted for spectroscopy, because these quasars are below the flux limit of the SDSS quasar catalog ($i < 19.1$ for quasars in this region of color space). The brighter member of Q1635+267 is above the flux limit, but this area of sky has only been imaged and has yet to be spectroscopically observed. However, both members of this pair are members of the faint photometric catalog, and indeed, this pair was selected as a candidate by our photometric selection. Both members of the binary HS 1216+5032 (Hagen et al. 1996) received SDSS fibers, so this binary is a member of our overlap sample. The brighter of the two members of the famous double quasar Q2345+007 received an SDSS fiber, and this pair was selected as a pair candidate by our χ^2 algorithm. Of the two binaries that were not recovered, Q1343+2650 was missed

[18] Although the fiber collision limit is $55''$, for operational purposes we take it to be $60''$ to give a small buffer from the actual limit, where the fiber tiling may still be imperfect.

[19] Available at http://cfa-www.harvard.edu/castles.

TABLE 1
PREVIOUSLY KNOWN BINARY QUASARS IN THE SDSS FOOTPRINT

Name	z	$\Delta\theta$	$R_{\rm prop}$	$\lvert\Delta v\rvert$	i_1	i_2	χ^2	Sample	Notes
SDSS J1120+6711	1.49	1.5	9.0	<100	18.49	19.57	...	Lens	1
Q1120+0195	1.47	6.5	39.6	630	15.61	20.26	20.6	...	2
HS 1216+5032	1.46	9.1	55.1	50	16.76	18.31	534.1	Overlap	3
Q1343+2650	2.03	9.2	55.4	200	19.14	19.97	113.7	...	4
LBQS 1429−008	2.08	5.1	30.8	260	17.40	20.74	4.3	χ^2	5
2QZ J1435+0008	2.38	33.2	194.8	760	19.90	20.56	7.0	χ^2	6
Q1635+267	1.96	3.9	23.2	30	19.04	20.26	7.7	Photo	7
SDSS J2336−0107	1.29	1.7	10.0	240	19.26	18.94	...	Lens	8
Q2345+007	2.16	7.1	42.4	480	18.68	20.45	0.3	χ^2	9

NOTES.—The redshift of the binary quasar is z, $\Delta\theta$ is the angular separation, R is the proper transverse separation, $|\Delta v|$ is the velocity difference between the two quasars in km s^{-1}, i_1 and i_2 are extinction-corrected i-band magnitudes of the brighter and fainter quasar, respectively, and χ^2 is the value of our color similarity statistic, computed only for pairs with $\Delta\theta > 3''$. The column labeled "Sample" indicates which of our selection algorithms recovered the binary. (1) SDSS binary quasar (Pindor et al. 2006). (2) Q1120+0195 is also named PHL 1222 and UM 144 (Meylan & Djorgovski 1989). (3) Spectra of both quasars are in the SDSS sample (Hagen et al. 1996). (4) Both quasars are below the flux limit of the quasar SDSS (Crampton et al. 1988). (5) Hewett et al. (1989). (6) Miller et al. (2004). (7) This region of sky has been imaged by the SDSS but not yet spectroscopically observed. Both quasars are members of the faint photometric quasar sample (Sramek & Weedman 1978). (8) SDSS binary quasar (Gregg et al. 2002). (9) Weedman et al. (1982).

because it was below the SDSS flux limits, and the quasar pair Q1120+0195 (Meylan & Djorgovski 1989) was missed because its χ^2 of 20.6 is just above the cutoff $\chi^2 < 20$ of the "χ^2" selection algorithm.

4. SPECTROSCOPIC OBSERVATIONS

Candidates in our lens, χ^2, and photometric samples require follow-up spectroscopy to confirm the quasar pair hypothesis, which we describe in this section. The SDSS images of the candidate quasar pairs and the spectrum of the quasar with an SDSS or 2QZ spectrum were visually inspected to reject bad imaging data and possible spectroscopic misidentifications. Color-color diagrams for each candidate were also visually inspected, and pairs for which the companion object overlaps the stellar locus (see, e.g., Richards et al. 2001a) were given a lower priority.

The result of a successful follow-up observation of a quasar pair candidate falls into one of four categories: (1) a quasar-quasar pair at the same redshift, (2) a projected pair of quasars at different redshifts, (3) a quasar-star pair, or (4) a star-star pair (for the photometric catalog). As an operational definition, we consider quasar pairs with velocity differences of $|\Delta v| \leq 2000$ km s^{-1} to be at the same redshift, since this brackets the range of velocity differences caused by both peculiar velocities, which could be as large as $\sim$500 km s^{-1} if the binary quasars reside in rich environments, and redshift uncertainties caused by blueshifted broad lines ($\sim$1500 km s^{-1}; Richards et al. 2002a).

Spectra of the vast majority of our quasar pair candidates were obtained with the Astrophysical Research Consortium (ARC) 3.5 m telescope at the APO, during a number of nights between 2003 March and 2005 January. In addition, two of the binary quasars in our sample were confirmed at other telescopes: SDSS J1600+0000 was confirmed at the ESO 3.58 m New Technology Telescope, and SDSS J1028+3929 was discovered at the Hobby-Eberly Telescope. Higher signal-to-noise ratio spectra of five of the binary quasars in our sample were obtained at the 10 m Keck I and Keck II telescopes.

For the ARC 3.5 m observations, we used the Double Imaging Spectrograph, a double spectrograph with a transition wavelength of 5350 Å between the blue and red side. The observations were taken with low-resolution gratings, with a dispersion of 2.4 Å pixel^{-1} in the blue side and 2.3 Å pixel^{-1} on the red side, and a resolution of roughly 2 pixels. A 1.″5 slit was used, and we oriented the slit at the position angle between the two quasars so that both members of the pair could be observed simultaneously. The final spectrum covered the wavelength range of 3800–10000 Å. Observations of a variety of optical spectrophotometric standards (Oke & Gunn 1983) provided flux calibration; however, most of the candidates were not observed under photometric conditions, nor were they observed with the slit oriented at the parallactic angle. Exposure times ranged from 1200 s for candidates with $i \sim 18$ to 2400 s for the faintest candidates, $i \sim 20.8$.

Higher signal-to-noise ratio spectra were obtained on the Keck I and Keck II telescopes. Both components of the quasar pairs SDSS J0955+6045, SDSS J1010+0416, and SDSS J1719+2549 were obtained on UT 2003 February 5–6 using the Echelle Spectrograph and Imager (ESI; Epps & Miller 1998) on the Keck II telescope. Spectra of the pair SDSS J0248+0009 were obtained on UT 1999 October 17 using the Low Resolution Imaging Spectrograph (LRIS) on Keck II (Oke et al. 1995) (before LRIS was commissioned as a double spectrograph), and SDSS J0048−1051 was observed on UT 2003 September 27 using the LRIS Double Spectrograph on the Keck I telescope.

All the data were reduced using standard procedures in the IRAF[20] package, supplemented by IDL routines borrowed from the SDSS spectroscopic reduction software and adapted to the different instruments. Quasar redshifts were determined by cross-correlating the quasar spectra with the first four eigenspectra of a principal component decomposition of the SDSS quasar sample (D. J. Schlegel et al. 2006, in preparation).

5. BINARY QUASAR SAMPLE

In this section we present a sample of 221 new quasar pairs with transverse separations $R_{\rm prop} < 1\ h^{-1}$ Mpc over the redshift range $0.5 \leq z \leq 3.0$. Of these, 65 have angular separations $\theta \leq 60''$, i.e., below the SDSS fiber collision scale. Our 26 new binaries with transverse proper separations $R_{\rm prop} < 50\ h^{-1}$ kpc ($\theta < 10''$) more than double the number of known binary quasars with separations this small. Table 2 lists the relevant quantities for 33 binaries with $3'' < \theta \leq 60''$ discovered from our χ^2

[20] IRAF is distributed by the National Optical Astronomy Observatory, which is operated by the Association of Universities for Research in Astronomy, Inc., under cooperative agreement with the National Science Foundation.

TABLE 2

BINARY QUASARS WITH SEPARATIONS $3'' < \Delta\theta < 60''$ DISCOVERED FROM FOLLOW-UP OBSERVATIONS

Name	R.A. (J2000.0)	Decl. (J2000.0)	u	g	r	i	z	$\Delta\theta$	z	Δv	$R_{\rm prop}$	χ^2	Sample
SDSS J0048−1051A	00 48 00.77	−10 51 48.6	20.99	20.52	20.18	19.94	19.91	3.6	1.56	<200	22.1	5.8	χ^2
SDSS J0048−1051B	00 48 00.96	−10 51 46.2	20.39	20.04	19.70	19.30	19.28						
SDSS J0054−0946A	00 54 08.47	−09 46 38.3	18.17	17.90	17.71	17.51	17.31	14.1	2.13	−1600	84.5	17.5	χ^2
SDSS J0054−0946B	00 54 08.04	−09 46 25.7	20.87	20.70	20.37	20.11	19.74						
SDSS J0117+3153A[a]	01 17 08.39	+31 53 38.7	21.20	20.42	20.32	20.39	20.10	11.3	2.13	1170	65.3	2.7	χ^2
SDSS J0117+3153B[a]	01 17 07.52	+31 53 41.2	20.41	19.77	19.66	19.66	19.43						
SDSS J0201+0032A	02 01 43.49	+00 32 22.7	19.99	19.39	19.47	19.41	19.19	19.0	2.30	−520	112.4	10.8	χ^2
SDSS J0201+0032B	02 01 42.25	+00 32 18.5	20.80	20.30	20.14	20.12	19.92						
SDSS J0248+0009A	02 48 20.80	+00 09 56.7	19.44	19.24	19.23	18.98	19.00	6.9	1.64	<200	41.9	8.8	χ^2
SDSS J0248+0009B	02 48 21.26	+00 09 57.3	20.77	20.71	20.74	20.57	20.39						
SDSS J0332−0722A	03 32 38.38	−07 22 15.9	20.24	20.29	20.00	19.78	19.63	18.1	2.10	960	108.4	5.0	Photo
SDSS J0332−0722B	03 32 37.19	−07 22 19.6	20.63	20.57	20.22	19.96	19.70						
SDSS J0846+2749A	08 46 31.77	+27 49 21.9	19.55	19.57	19.66	19.49	19.26	18.8	2.12	−490	112.4	14.3	χ^2
SDSS J0846+2749B	08 46 30.38	+27 49 18.1	19.82	19.88	19.82	19.71	19.55						
SDSS J0939+5953A	09 39 48.78	+59 53 48.7	20.40	19.85	19.80	19.79	19.45	32.6	2.53	290	189.4	9.3	χ^2
SDSS J0939+5953B	09 39 46.56	+59 53 20.7	19.31	18.67	18.57	18.56	18.42						
SDSS J0955+6045A	09 55 24.37	+60 45 51.0	20.84	20.37	20.29	20.25	20.34	18.6	0.72	460	95.5	10.8	χ^2
SDSS J0955+6045B	09 55 25.37	+60 45 33.8	20.68	20.65	20.62	20.72	20.30						
SDSS J0959+5449A	09 59 07.46	+54 49 06.7	20.26	20.06	19.95	19.76	19.73	3.9	1.95	200	23.8	18.9	Photo
SDSS J0959+5449B	09 59 07.05	+54 49 08.4	20.48	20.61	20.43	20.28	19.82						
SDSS J1010+0416A	10 10 04.98	+04 16 36.2	20.18	20.08	20.00	19.87	20.08	17.2	1.51	<200	104.3	6.5	χ^2
SDSS J1010+0416B	10 10 04.37	+04 16 21.6	20.29	20.19	20.03	19.87	19.94						
SDSS J1014+0920A	10 14 11.43	+09 20 47.7	19.95	19.14	19.12	18.92	18.73	22.0	2.29	<200	129.8	11.7	χ^2
SDSS J1014+0921B	10 14 10.29	+09 21 01.7	20.81	20.27	20.25	20.13	19.79						
SDSS J1028+3929A	10 28 43.67	+39 29 36.9	19.96	19.90	19.95	19.57	19.49	7.5	1.89	−1030	45.6	6.4	Photo
SDSS J1028+3929B	10 28 44.30	+39 29 34.8	20.92	20.81	20.91	20.60	20.66						
SDSS J1034+0701A	10 34 51.47	+07 01 21.2	19.86	19.47	18.94	19.04	19.08	3.1	1.25	850	18.7	9.7	χ^2
SDSS J1034+0701B	10 34 51.38	+07 01 24.0	21.20	21.26	21.08	20.89	20.99						
2QZ J1056−0059A	10 56 44.89	−00 59 33.4	20.16	19.92	19.89	19.80	19.59	7.2	2.13	−350	43.1	6.7	χ^2
SDSS J1056−0059B	10 56 45.25	−00 59 38.1	20.76	20.78	20.59	20.58	20.33						
SDSS J1123+0037A	11 23 10.96	+00 37 45.2	19.02	19.03	18.90	18.98	19.08	56.3	1.17	−330	332.1	6.0	χ^2
SDSS J1123+0037B	11 23 07.21	+00 37 45.7	20.26	20.29	20.10	20.12	20.22						
SDSS J1225+5644A	12 25 45.73	+56 44 40.7	20.05	19.28	19.44	19.35	19.07	6.0	2.38	970	35.4	20.7	Photo
SDSS J1225+5644B	12 25 45.24	+56 44 45.1	21.08	20.52	20.50	20.35	19.80						
SDSS J1254+6104A	12 54 21.98	+61 04 22.0	19.24	19.06	19.01	18.92	18.74	17.6	2.05	−1010	105.6	11.4	χ^2
SDSS J1254+6104B	12 54 20.52	+61 04 36.0	19.67	19.56	19.47	19.28	19.14						
SDSS J1259+1241A	12 59 55.62	+12 41 53.8	20.33	19.99	19.93	19.74	19.53	3.6	2.19	−840	21.2	6.0	Photo
SDSS J1259+1241B	12 59 55.46	+12 41 51.0	20.22	19.90	19.87	19.79	19.56						
SDSS J1303+5100A	13 03 26.17	+51 00 47.5	20.46	20.33	20.28	20.05	20.03	3.8	1.68	220	23.0	4.0	Photo
SDSS J1303+5100B	13 03 26.13	+51 00 51.3	20.87	20.60	20.66	20.38	20.59						
SDSS J1310+6208A	13 10 37.89	+62 08 21.6	18.87	18.77	18.63	18.57	18.35	46.9	2.06	−1850	281.7	10.8	χ^2
SDSS J1310+6208B	13 10 31.96	+62 08 43.5	20.65	20.49	20.35	20.15	20.12						
SDSS J1337+6012A	13 37 13.13	+60 12 06.7	18.68	18.57	18.56	18.34	18.42	3.1	1.73	−610	18.9	0.6	χ^2
SDSS J1337+6012B	13 37 13.08	+60 12 09.8	20.15	20.01	20.03	19.66	19.80						
SDSS J1349+1227A	13 49 29.84	+12 27 07.0	17.92	17.76	17.71	17.46	17.45	3.0	1.72	<200	18.3	12.9	χ^2
SDSS J1349+1227B	13 49 30.00	+12 27 08.8	19.50	19.26	19.10	18.74	18.60						
SDSS J1400+1232A	14 00 52.07	+12 32 35.2	20.41	20.28	20.27	20.13	19.88	14.6	2.05	1470	87.7	0.6	Photo
SDSS J1400+1232B	14 00 52.56	+12 32 48.0	20.54	20.42	20.45	20.27	19.99						
SDSS J1405+4447A	14 05 01.94	+44 47 59.9	18.68	18.14	17.93	17.86	17.66	7.4	2.23	1870	44.2	3.2	χ^2
SDSS J1405+4447B	14 05 02.41	+44 47 54.4	20.61	20.12	19.96	19.89	19.60						
SDSS J1409+3919A	14 09 53.74	+39 19 60.0	20.31	20.24	20.14	20.06	19.78	6.8	2.08	480	40.7	3.9	Photo
SDSS J1409+3919B	14 09 53.88	+39 19 53.4	20.89	20.92	20.87	20.67	20.31						
SDSS J1530+5304A	15 30 38.56	+53 04 04.2	20.86	20.54	20.42	20.13	20.06	4.1	1.53	230	25.0	8.8	Photo
SDSS J1530+5304B	15 30 38.82	+53 04 00.8	20.67	20.66	20.53	20.31	20.21						
SDSS J1546+5134A	15 46 10.55	+51 34 29.5	22.34	20.57	20.31	20.20	20.29	42.2	2.95	−1450	236.0	12.4	χ^2
SDSS J1546+5134B	15 46 14.24	+51 34 05.0	20.64	19.43	19.10	18.91	18.88						
SDSS J1629+3724A	16 29 02.59	+37 24 30.8	19.47	19.26	19.10	19.16	19.06	4.4	0.92	<200	24.5	15.9	χ^2
SDSS J1629+3724B	16 29 02.63	+37 24 35.2	19.50	19.41	19.28	19.38	19.31						
SDSS J1719+2549A	17 19 46.66	+25 49 41.2	20.17	19.93	19.90	19.85	19.61	14.7	2.17	−220	87.5	6.4	χ^2
SDSS J1719+2549B	17 19 45.87	+25 49 51.3	20.08	19.74	19.65	19.65	19.46						
SDSS J1723+5904A	17 23 17.42	+59 04 46.8	19.40	19.04	18.95	18.69	18.76	3.7	1.60	−830	22.7	3.0	χ^2
SDSS J1723+5904B	17 23 17.30	+59 04 43.2	21.24	20.43	20.46	20.18	20.20						

TABLE 2—*Continued*

Name	R.A. (J2000.0)	Decl. (J2000.0)	u	g	r	i	z	$\Delta\theta$	z	Δv	$R_{\rm prop}$	χ^2	Sample
SDSS J2128−0617A	21 28 57.38	−06 17 50.9	19.84	19.66	19.87	19.80	19.68	8.3	2.07	−290	49.7	15.7	Photo
SDSS J2128−0617B	21 28 57.74	−06 17 57.2	20.03	19.74	20.12	19.92	19.63						
SDSS J2214+1326A	22 14 27.03	+13 26 57.0	20.39	20.19	20.19	19.96	19.60	5.8	2.00	−690	35.2	19.4	Photo
SDSS J2214+1326B	22 14 26.79	+13 26 52.3	20.65	20.41	20.26	19.98	19.82						
SDSS J2220+1247A	22 20 30.26	+12 47 33.5	20.11	20.03	20.00	19.88	19.78	15.9	1.99	1600	95.5	43.0	Photo
SDSS J2220+1247B	22 20 29.53	+12 47 45.1	20.92	20.85	20.72	20.34	20.21						

NOTES.—Units of right ascension are hours, minutes, and seconds, and units of declination are degrees, arcminutes, and arcseconds. Quasars labeled "A" are the members of the SDSS or 2QZ spectroscopic quasar catalog. Quasars discovered from follow-up spectroscopy are designated as "B." For pairs discovered from the photometric catalog, "A" designates the brighter of the two quasars. Extinction-corrected SDSS five-band PSF photometry is given in the columns u, g, r, i, and z. The redshift of quasar A is indicated by the second "z" column, $\Delta\theta$ is the angular separation in arcseconds, Δv is the velocity of quasar B relative to quasar A in km s^{-1}, $R_{\rm prop}$ is the transverse proper separation in h^{-1} kpc, and χ^2 is the value of our color similarity statistic. The column labeled "Sample" indicates the selection algorithm used to find the binary. Table 2 is also available in machine-readable form in the electronic edition of the *Astronomical Journal*.

[a] The binary quasar SDSS J0117+3153 was discovered after this paper was submitted for publication. It is published here for completeness; however, it is not used in the clustering analyses discussed in the text.

and photometric samples. The last column indicates the algorithm that was used to select the binary. The binaries with $\theta \leq 3''$ discovered from our lens sample are shown in Table 3, and the overlap and spectroscopic binaries found by searching for pairs in the SDSS + 2QZ quasar catalog are shown in Table 4. Table 5 gives a summary of the number of binary quasars selected by each algorithm described in § 3. For completeness, the Appendix includes tables of projected pairs of quasars at different redshifts, as well as projected quasar-star pairs.

The distribution of redshifts and proper transverse separations probed by these binary quasars is illustrated by the scatter plot in Figure 3. The upside-down triangles show members of the lens sample, the squares show members of the photometric sample, and the upright triangles show the χ^2 sample. The open circles show members of the overlap sample, and the smaller dots show pairs in the spectroscopic sample. The dashed curve shows the proper transverse distance corresponding to $\theta = 3''$, which divides the lens sample from the other samples, and the dotted line indicates the distance corresponding to $\theta = 60''$, above the fiber collision limit so that pairs can be found in the spectroscopic quasar catalog. It should be noted that the distribution of symbols in Figure 3 reflects some biases in our observational program. In particular, we tended to observe small-separation pairs first, and we were much more likely to observe candidates with $z > 2$, because quasar pairs at these redshifts are of interest for studying the Lyα forest (Lidz et al. 2003; Hennawi 2005).

We next discuss the possibility that some of the quasar pairs in this sample are strong gravitational lenses rather than binaries. After showing spectra of some of the more notable binaries, we define a subsample of binaries selected homogeneously that we use in our analysis of small-scale quasar clustering in § 6.

5.1. *Contamination by Gravitational Lenses*

It is possible that some of the quasar pairs with image splittings $\lesssim 15''$ in our sample could be wide-separation strong gravitational lenses rather than binary quasars. Indeed, the recently discovered quadruply imaged lensed quasar SDSS J1004+4112 (Inada et al. 2003b; Oguri et al. 2004), with a maximum image separation of $14\farcs6$, was discovered as part of our follow-up campaign to discover quasar pairs, as were two new gravitational

TABLE 3

BINARY QUASARS WITH $\Delta\theta < 3''$ DISCOVERED FROM LENS SELECTION

Name	R.A. (J2000.0)	Decl. (J2000.0)	u	g	r	i	z	$\Delta\theta$	z	Δv	$R_{\rm prop}$
SDSS J0740+2926A	07 40 13.45	+29 26 48.4	18.61	18.46	18.30	18.42	18.48	2.6	0.98	230	15.0
SDSS J0740+2926B	07 40 13.43	+29 26 45.7	19.98	19.67	19.50	19.68	20.03				
SDSS J1035+0752A	10 35 19.37	+07 52 58.0	19.17	19.13	18.97	19.03	19.14	2.7	1.22	270	15.8
SDSS J1035+0752B	10 35 19.23	+07 52 56.4	20.62	20.42	19.98	19.84	19.84				
SDSS J1124+5710A	11 24 55.24	+57 10 57.0	19.34	18.66	18.83	18.65	18.44	2.2	2.31	−540	12.7
SDSS J1124+5710B	11 24 55.44	+57 10 58.4	20.31	19.83	19.52	19.52	19.42				
SDSS J1138+6807A	11 38 09.21	+68 07 38.8	18.28	17.98	17.87	17.89	17.78	2.6	0.77	840	13.7
SDSS J1138+6807B	11 38 08.89	+68 07 36.9	20.31	19.74	19.76	19.72	19.58				
SDSS J1508+3328A	15 08 42.21	+33 28 02.6	17.88	17.78	17.81	17.97	17.86	2.9	0.88	<200	16.0
SDSS J1508+3328B	15 08 42.22	+33 28 05.5	20.56	20.36	20.15	20.56	19.71				
SDSS J1600+0000A[a]	16 00 15.50	+00 00 45.5	19.23	19.11	18.84	18.95	19.08	1.9	1.01	−660	10.6
SDSS J1600+0000B[a]	16 00 15.59	+00 00 46.9	...	...	≈21	≈21	...				

NOTES.—Units of right ascension are hours, minutes, and seconds, and units of declination are degrees, arcminutes, and arcseconds. Quasars labeled "A" are the members of the SDSS spectroscopic quasar catalog. Quasars discovered from follow-up spectroscopy are designated as "B." Extinction-corrected SDSS five-band PSF photometry is given in the columns u, g, r, i, and z. These magnitudes are estimated from the deblending algorithm of the main SDSS photometric pipeline (Stoughton et al. 2002) (except for SDSS J1600+0000; see below in this note). The redshift of the SDSS quasar is given by the second "z" column, $\Delta\theta$ is the angular separation in arcseconds, Δv is the velocity of quasar B relative to quasar A in km s^{-1}, and $R_{\rm prop}$ is the transverse proper separation in h^{-1} kpc. Table 3 is also available in machine-readable form in the electronic edition of the *Astronomical Journal*.

[a] The pair SDSS J1600+0000A and SDSS J1600+0000B was not deblended by the photometric pipeline because the separation is too small. The magnitudes of SDSS J1600+0000A have contributions from both members of the pair, and the approximate r- and i-band magnitudes of NTT J1600+0000B were measured from follow-up NTT imaging of this system.

TABLE 4

BINARY QUASARS DISCOVERED IN OVERLAPPING PLATES AND THE SDSS + 2QZ CATALOG

Name	R.A. (J2000.0)	Decl. (J2000.0)	u	g	r	i	z	$\Delta\theta$	z	Δv	$R_{\rm prop}$	χ^2
SDSS J0012+0052A	00 12 01.88	+00 52 59.7	21.53	20.82	20.33	19.83	19.63	16.0	1.63	1590	97.3	59.8
SDSS J0012+0053B	00 12 02.35	+00 53 14.1	21.03	20.82	20.51	20.22	20.10					
SDSS J0117+0020A	01 17 58.84	+00 20 21.5	17.96	17.67	17.82	17.79	17.99	44.5	0.61	−260	212.9	34.1
SDSS J0117+0021B	01 17 58.00	+00 21 04.1	20.26	20.01	20.13	19.86	19.89					
SDSS J0141+0031A	01 41 11.63	+00 31 45.9	20.23	20.19	20.11	19.87	19.96	42.9	1.89	1140	259.2	2.9
SDSS J0141+0031B	01 41 10.41	+00 31 07.1	20.76	20.59	20.50	20.29	20.20					
SDSS J0245−0113A	02 45 12.08	−01 13 14.0	20.56	19.85	19.56	19.47	19.33	4.5	2.46	−190	26.3	17.0
SDSS J0245−0113B	02 45 11.90	−01 13 17.6	21.14	20.57	20.45	20.38	20.11					
SDSS J0258−0003A	02 58 15.55	−00 03 34.2	18.93	18.93	18.66	18.66	18.74	29.4	1.32	240	176.6	32.9
SDSS J0258−0003B	02 58 13.66	−00 03 26.5	19.67	19.89	19.66	19.75	19.71					
SDSS J0259+0048A	02 59 59.69	+00 48 13.7	19.63	19.26	19.22	19.33	19.10	19.6	0.89	830	108.1	1914.2
SDSS J0300+0048B*	03 00 00.57	+00 48 28.0	19.47	19.01	16.51	16.37	16.05					
SDSS J0350−0031A	03 50 53.29	−00 31 14.7	20.35	20.17	19.45	18.99	18.62	45.5	2.00	−920	273.8	492.9
SDSS J0350−0032B	03 50 53.05	−00 32 00.1	19.66	19.40	19.32	19.29	19.16					
SDSS J0743+2054A	07 43 37.29	+20 54 37.1	20.06	19.86	19.77	19.51	19.43	35.5	1.56	640	215.5	15.9
SDSS J0743+2055B	07 43 36.85	+20 55 12.1	20.36	20.08	20.04	19.90	19.94					
SDSS J0747+4318A	07 47 59.02	+43 18 05.4	19.52	19.24	19.21	18.89	18.75	9.2	0.50	150	39.9	6.3
SDSS J0747+4318B	07 47 59.66	+43 18 11.5	19.79	19.45	19.36	19.11	18.99					
SDSS J0824+2357A	08 24 40.61	+23 57 09.9	18.72	18.51	18.69	18.58	18.59	14.9	0.54	−170	67.0	13.2
SDSS J0824+2357B	08 24 39.83	+23 57 20.3	19.00	18.67	18.88	18.70	18.72					
SDSS J0856+5111A	08 56 25.63	+51 11 37.4	18.90	18.52	18.64	18.45	18.51	21.8	0.54	60	98.2	138.9
SDSS J0856+5111B	08 56 26.71	+51 11 18.2	20.03	19.55	19.42	19.17	19.19					
SDSS J0909+0002A	09 09 24.01	+00 02 11.0	16.65	16.68	16.61	16.39	16.34	15.0	1.87	1700	90.6	28.0
SDSS J0909+0002B	09 09 23.13	+00 02 04.0	20.08	20.06	20.11	19.97	19.82					
SDSS J0955+0616A	09 55 56.38	+06 16 42.5	17.79	18.07	17.84	17.81	17.86	44.0	1.28	−1040	263.3	38.6
SDSS J0955+0617B	09 55 59.03	+06 17 01.9	20.35	20.29	20.11	20.21	20.29					
SDSS J1032+0140A	10 32 44.65	+01 40 20.5	18.93	18.86	18.84	18.76	18.86	55.1	1.46	−1580	333.5	16.0
2QZ J1032+0139B	10 32 43.17	+01 39 30.0	20.50	20.46	20.27	20.15	20.21					
SDSS J1103+0318A	11 03 57.72	+03 18 08.3	18.35	18.36	18.30	18.10	17.96	57.3	1.94	−1730	345.7	41.5
SDSS J1104+0318B	11 04 01.49	+03 18 17.5	19.08	19.04	19.12	19.02	18.97					
SDSS J1107+0033A	11 07 25.70	+00 33 53.9	18.98	18.94	18.84	18.51	18.42	24.8	1.88	280	150.1	22.9
2QZ J1107+0034B	11 07 27.08	+00 34 07.6	20.01	20.04	20.05	19.84	19.80					
SDSS J1116+4118A	11 16 11.74	+41 18 21.5	20.35	18.53	18.16	17.94	17.96	13.8	2.99	890	76.8	28.4
SDSS J1116+4118B	11 16 10.69	+41 18 14.4	21.33	19.44	19.17	19.03	19.03					
SDSS J1134+0849A	11 34 57.74	+08 49 35.3	19.30	19.10	19.01	18.83	18.85	27.1	1.53	−390	164.4	6.4
SDSS J1134+0849B	11 34 59.38	+08 49 23.3	19.65	19.50	19.34	19.11	19.13					
2QZ J1146−0124A	11 46 52.97	−01 24 46.4	20.54	20.23	20.17	19.93	19.65	28.5	1.98	−490	172.0	26.0
2QZ J1146−0124B	11 46 51.19	−01 24 56.3	20.53	20.46	20.52	20.35	20.24					
SDSS J1152−0030A	11 52 40.53	−00 30 04.3	18.95	18.80	18.93	18.86	18.80	29.3	0.55	740	132.8	23.1
2QZ J1152−0030B	11 52 40.10	−00 30 32.9	20.32	20.12	20.16	19.99	20.16					
SDSS J1207+0115A	12 07 00.97	+01 15 39.4	19.03	18.94	18.84	18.87	18.85	35.4	0.97	−260	200.1	3.5
2QZ J1207+0115B	12 07 01.40	+01 15 04.7	20.62	20.40	20.30	20.37	20.36					
2QZ J1217+0006A	12 17 36.18	+00 06 57.4	19.96	19.93	20.06	19.76	19.62	51.8	1.78	−200	314.0	13.5
2QZ J1217+0006B	12 17 35.03	+00 06 08.6	19.17	19.30	19.32	19.05	19.17					
2QZ J1217+0055A	12 17 36.95	+00 55 22.7	20.33	20.24	20.12	20.23	19.84	40.5	0.90	−60	224.7	18.3
2QZ J1217+0055B	12 17 34.25	+00 55 22.2	20.25	19.92	19.78	19.82	19.98					
SDSS J1226−0112A	12 26 24.09	−01 12 34.5	17.47	17.39	17.23	17.27	17.28	50.6	0.92	100	282.4	22.8
2QZ J1226−0113B	12 26 25.58	−01 13 19.9	19.74	19.82	19.75	19.79	19.53					
SDSS J1300−0156A	13 00 45.56	−01 56 31.8	18.26	18.26	18.14	17.88	17.90	44.5	1.62	480	270.7	37.6
2QZ J1300−0157B	13 00 44.52	−01 57 13.5	19.81	19.72	19.73	19.59	19.70					
2QZ J1328−0157A	13 28 30.14	−01 57 32.8	19.86	19.49	19.52	19.55	19.42	52.6	2.37	−890	309.2	26.8
2QZ J1328−0157B	13 28 33.64	−01 57 27.9	20.46	19.92	19.78	19.77	19.75					
2QZ J1354−0108A	13 54 40.40	−01 08 45.4	19.48	19.54	19.46	19.29	19.21	55.5	1.99	740	334.2	37.1
2QZ J1354−0107B	13 54 39.97	−01 07 50.3	20.40	20.13	19.99	19.85	19.64					

NOTES.—Units of right ascension are hours, minutes, and seconds, and units of declination are degrees, arcminutes, and arcseconds. The brighter of the two quasars is designated "A," except for SDSS-2QZ pairs, for which the SDSS quasar is designated "A." Extinction-corrected SDSS five-band PSF photometry is given in the columns u, g, r, i, and z. The redshift of quasar A is indicated by the second "z" column, $\Delta\theta$ is the angular separation in arcseconds, Δv is the velocity of quasar B relative to quasar A in km s^{-1}, $R_{\rm prop}$ is the transverse proper separation in h^{-1} kpc, and χ^2 is the value of our color similarity statistic. We publish all quasars with proper transverse separations $R_{\rm prop} < 1\ h^{-1}$ Mpc; however, only those with $\theta < 60''$ are listed in this table. The asterisk indicates that quasar SDSS J0300+0048B has a large broad absorption line trough, which explains the very large $\chi^2 = 1914.2$ for this pair. Table 4 is published in its entirety in the electronic edition of the *Astronomical Journal*. A portion is shown here for guidance regarding its form and content.

TABLE 5
SUMMARY OF BINARY QUASAR SAMPLE

Algorithm	Number of Binaries
Lens	6
χ^2	21
Photometric	12
Overlap	26
Spectroscopic	153

NOTES.—The right column is the number of binary quasars with $R_{\rm prop} < 1\ h^{-1}$ Mpc, selected by the various algorithms discussed in § 3 and plotted in Fig. 3.

lenses with separations $\gtrsim 3''$ (Oguri et al. 2005). We thus review the set of objective criteria that must be satisfied for a quasar pair to be classified as a binary or lens (Kochanek et al. 1999; Mortlock et al. 1999) and briefly discuss why we have concluded that the binary hypothesis is correct for our pairs.

A quasar pair can be positively confirmed as a binary if the spectra of the images are vastly different (see Gregg et al. 2002), if only one of the images is radio-loud (an O^2R pair, in the notation of Kochanek et al. [1999]), or if the quasars' hosts are detected and they are not clearly lensed. The sufficient conditions for a pair to be identified as a lens are the presence of more than two images in a lensing configuration, the measurement of a time delay between images, the detection of a plausible deflector, or the detection of lensed host galaxy emission.

For the majority of pairs in our sample, the APO discovery spectra have too low a signal-to-noise ratio to make convincing arguments for or against the lensing hypothesis based on spectral dissimilarity. The exceptions are the five binaries for which we have high signal-to-noise ratio Keck spectra (three from ESI and two from LRIS). We comment on the spectral similarity of these binaries below.

Although the *absence* of a deflector in images of a quasar pair does not, strictly speaking, confirm the binary hypothesis, it certainly makes it more plausible. For small-separation ($\Delta\theta \lesssim 3''$) gravitational lenses, the lens galaxies are rarely detected in the relatively shallow SDSS imaging. However, for the wider separation lenses with $\Delta\theta \gtrsim 3''$, such as SDSS J1004+4112 ($\Delta\theta_{\rm max} = 14\farcs62$, $z_{\rm lens} = 0.68$) or Q0957+561 ($\Delta\theta = 6\farcs2$, $z_{\rm lens} = 0.36$; Walsh et al. 1979), where the lens is a bright galaxy in a cluster or group, the lens galaxies *are* detected in the SDSS imaging, although it is quite possible that fainter high-redshift lens galaxies or clusters in other wide-separation lens systems would go undetected.

Using the University of Hawaii 2.2 m telescope, we have taken deeper optical ($i \lesssim 24$, $z \lesssim 22$) or near-infrared images ($J \lesssim 22$, $H \lesssim 22$) of all the binaries in our sample with separations $\theta \leq 4''$ and of a subset of those with wider separations. None of the images showed lens galaxies in the foreground. For the wider $\theta > 4''$ pairs, the lensing hypothesis would require a very bright massive galaxy in a group or cluster. In particular, because the typical redshift range of our binaries is $z = 1.5$–2, the most probable lens redshifts would be in the range $z = 0.3$–0.7, which would likely have been detected in the SDSS imaging. Furthermore, these wide-separation, multiply imaged quasars are extremely rare (Hennawi et al. 2005); thus, we are confident that the pairs in our sample are all binaries.

5.2. *Sample Spectra of Binaries*

Keck ESI spectra of the three binaries SDSS J0955+6045, SDSS J1010+0416, and SDSS J1719+2549 are shown in Figure 4.

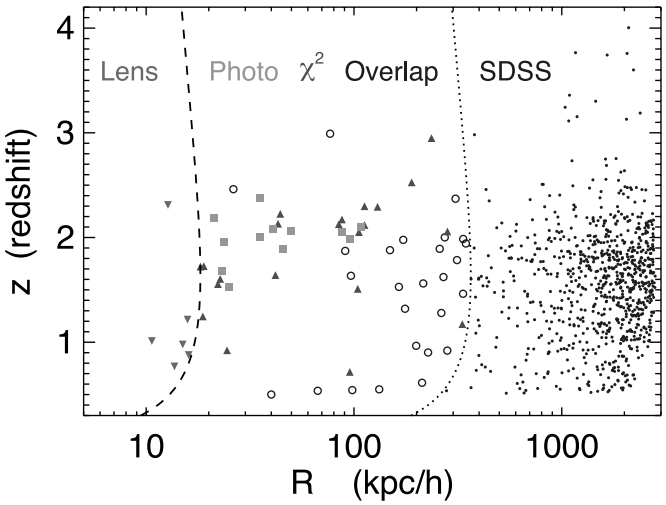

FIG. 3.—Range of redshifts and proper transverse separations probed by the binary quasars published in this work (see Tables 2–5). The dots show binary quasars identified in the SDSS spectroscopic sample. The region to the left of the dotted curve is excluded because of fiber collisions ($\theta < 60''$), with the exception of the binaries discovered from overlapping plates, which are indicated by the larger open circles. The upside-down triangles show members of the lens sample, the upright triangles are from the χ^2 sample, and the squares show binaries from the photometric sample. Because of the fiber collisions, the vast majority of small-separation ($R \lesssim 300\ h^{-1}$ kpc) pairs were discovered from our follow-up observations. The dashed curve indicates the transverse separation corresponding to $\theta = 3''$ below which binaries are found with our lens algorithm. Although we publish only pairs with separations $R_{\rm prop} < 1\ h^{-1}$ Mpc in this work, Fig. 3 shows all pairs in the SDSS + 2QZ catalog out to $3\ h^{-1}$ Mpc for the sake of illustration. [*See the electronic edition of the Journal for a color version of this figure.*]

The signal-to-noise ratios of these spectra are high enough that we can make arguments against the lensing hypothesis based on spectral dissimilarity. In particular, for SDSS J0955+6045 the narrow [O III] emission lines are significantly stronger in one of the quasars than the other. In SDSS J1010+0416, the C III] emission lines have a velocity offset of $\sim$2000 km s^{-1}, although this offset is less apparent in Mg II, which tends to be a better tracer of the systemic redshifts of quasars (Richards et al. 2002a). Finally, for SDSS J1719+2549 the peak-to-continuum flux ratios of the Mg II broad line differ by a factor of $\sim$1.5 between the two quasars.

Figure 5 shows Keck LRIS spectra of SDSS J0048−1051 (moderate resolution) and SDSS J0248+0009 (low resolution). For SDSS J0048−1051 the profiles of all the emission lines differ significantly, especially Mg II. For SDSS J0248+0009, the peak-to-continuum flux ratios differ significantly for C IV, C III], and Mg II. Figures 6 and 7 show SDSS and APO spectra of six other binaries in our sample.

5.3. *Clustering Subsample*

In this section we define a statistical subsample of binary quasars that we use to measure the quasar correlation function in § 6. In § 3 the various samples used to identify the binary quasars in Tables 2–4 were described. These various selection algorithms selected quasar pairs over different angular scales, with different limiting magnitudes and varying degrees of completeness. Here we combine these samples in a coherent way, which allows us to quantify their selection function. We pay special attention to the completeness of each sample used and the parent sample of quasars searched to define each sample.

For the clustering analysis we restrict attention to quasars in the redshift range $0.7 \leq z \leq 3.0$ with velocity differences $|\Delta v| <$ 2000 km s^{-1}. We use the lens, χ^2, overlap, and spectroscopic

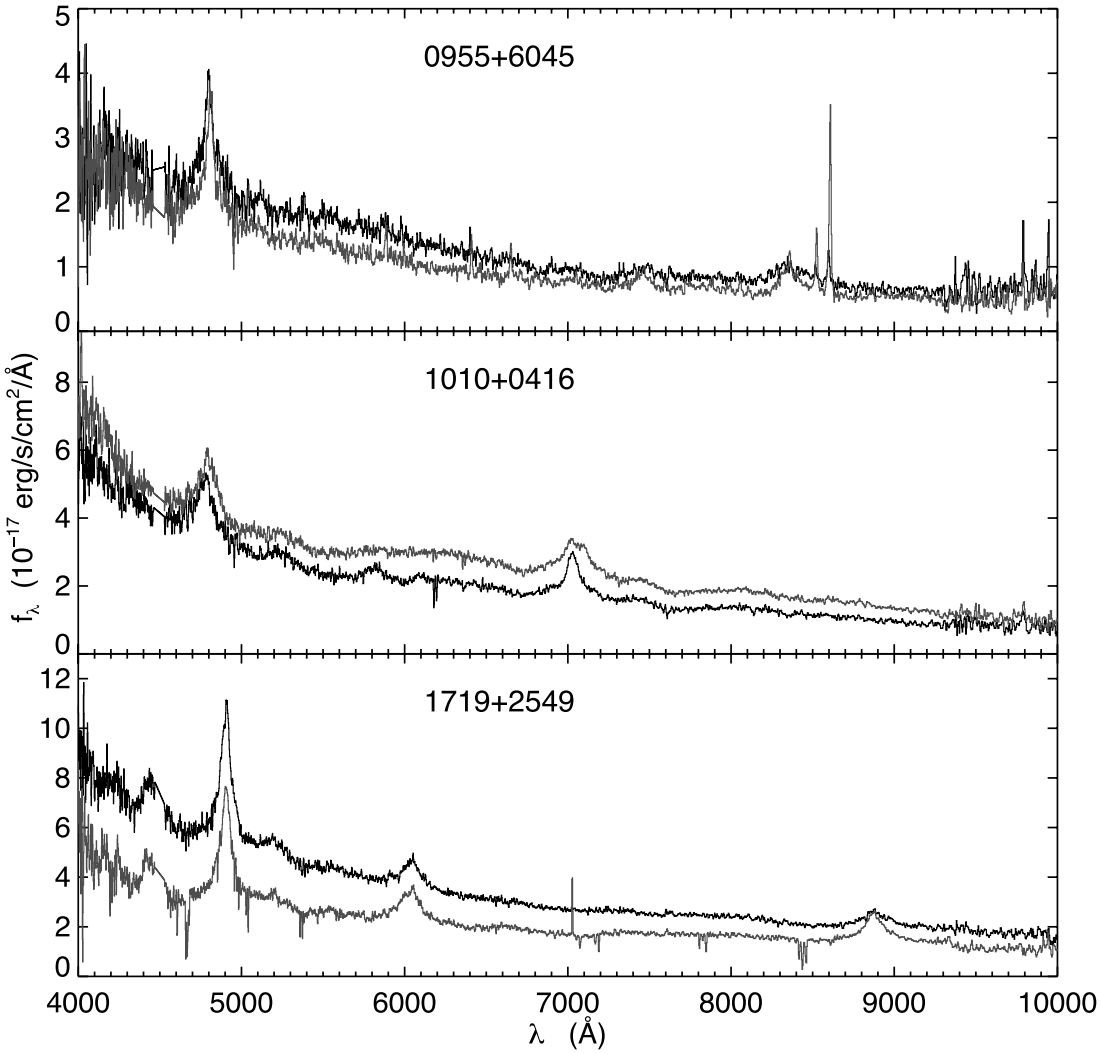

FIG. 4.—Keck ESI spectra of both members of three binary quasars. The top panel shows the binary SDSS J0955+6045 ($z = 0.72$, $\Delta\theta = 18\farcs6$, $R_{\rm prop} = 95.5\ h^{-1}$ kpc), the middle panel shows SDSS J1010+0416 ($z = 1.51$, $\Delta\theta = 17\farcs2$, $R_{\rm prop} = 104.3\ h^{-1}$ kpc), and the bottom panel shows SDSS J1719+2549 ($z = 2.17$, $\Delta\theta = 14\farcs7$, $R_{\rm prop} = 87.5\ h^{-1}$ kpc). The discontinuity in the spectra at 4500 Å is an artifact of a gap in the echelle orders. The ESI has a dispersion of 0.15–0.3 Å pixel^{-1} over a wavelength range of 4000–10500 Å. [*See the electronic edition of the Journal for a color version of this figure.*]

samples. Our approach is to stitch the samples together as a function of angle. The photometric quasar pairs are not in the SDSS + 2QZ catalog, so the selection function and completeness of these binaries are more difficult to quantify.

All pairs with $\theta \leq 3''$ come from the lens sample. The parent sample of quasars for this angular range is the 39,142 SDSS quasars to which we applied the lens algorithm. The completeness is the product of the *intrinsic* completeness of the lens algorithm (Pindor et al. 2003; Inada et al. 2003a) and the fraction of candidates that have had spectroscopic confirmation thus far in the survey.

For pairs in the range $3'' < \theta \leq 60''$ we use the χ^2 sample. Quasar pairs from the overlap sample that *also* meet the χ^2 selection criteria in equation (4) are included and can be thought of as follow-up observations that came for "free" from the overlapping plates. Of the 21 binaries with $0.7 \leq z \leq 3.0$ in the overlap sample, eight satisfy $\chi^2 < 20$ (see Table 4) and are included in the clustering subsample. The completeness of binary quasars in the range $3'' < \theta \leq 60''$ is the product of completeness of the χ^2 selection, $C(z|\chi^2 < 20)$, and the fraction of candidates observed thus far. The parent sample around which we searched with the χ^2 algorithm is the combined SDSS + 2QZ quasar sample of 59,608 quasars in the range $0.7 \leq z \leq 3.0$.

For separations $\theta > 60''$ we use pairs found in the SDSS spectroscopic catalog of 52,279 quasars. We restrict attention to the SDSS (rather than SDSS + 2QZ), because the completeness for detecting quasar companions is very high if we restrict attention to companions above the SDSS flux limit for low-redshift quasars. Vanden Berk et al. (2005) measured a completeness of $\sim$95% for quasars in the range $0.3 < z < 3.0$ with $i < 19.1$. Thus, we only include quasar pairs $\theta > 60''$ in our clustering sample provided that *at least one* member of the pair is brighter than this flux limit.

Finally, any of the previously known binaries listed in Table 1 that satisfied any of the criteria for the clustering subsample are also included. Thus, we include the binaries SDSS J1120+6711 and SDSS J2336−0107 as part of the lens sample, and LBQS 1429−0008, Q2345+007, and 2QZ J1435+0008 are included as part of our χ^2 sample.

Of the 65 quasar pairs with angular separations $\theta \leq 60''$ that we publish in this work, 35 are included in our clustering subsample along with five previously known binaries for a total of 40 subarcminute pairs. The distribution of redshifts and proper transverse separations of our clustering sample is illustrated by the scatter plot in Figure 8. The horizontal long-dashed lines

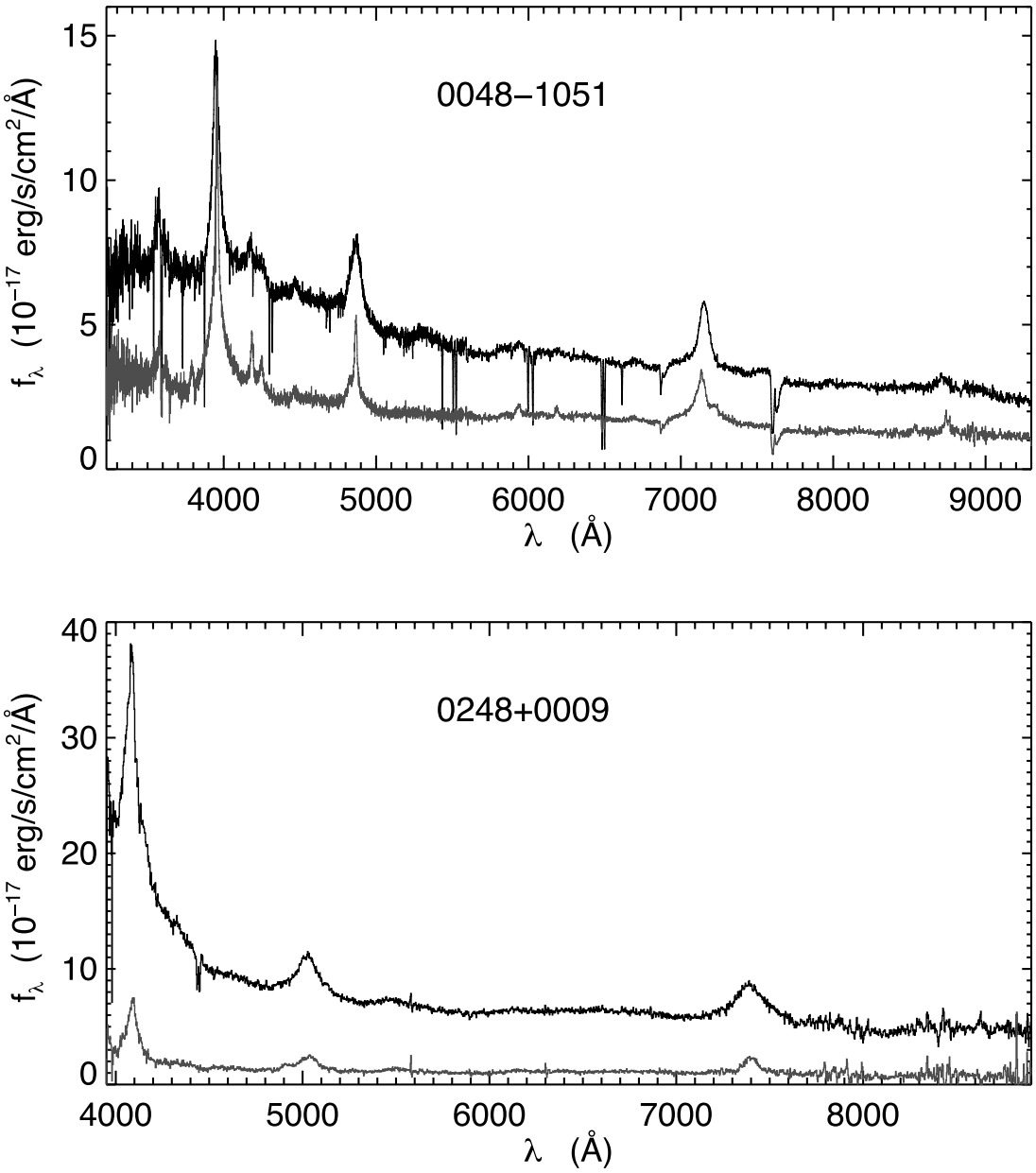

FIG. 5.—Keck spectra of two binary quasars. Spectral dissimilarity and the absence of a lensing galaxy in optical and near-IR follow-up imaging provide strong evidence that these are both binary quasars rather than gravitational lenses. *Top*: Keck LRIS moderate-resolution spectra of both members of the binary quasar SDSS J0048−1051 ($z = 1.56$, $\Delta\theta = 3\farcs6$, $R = 22.1\ h^{-1}$ kpc). The resolution is 0.63 Å pixel^{-1} for $\lambda < 5600$ Å and 1.86 Å pixel^{-1} for $\lambda > 5600$ Å. The absorption feature at 7600 Å is telluric. *Bottom*: Keck LRIS low-resolution (2.55 Å pixel^{-1}) spectra of both members of SDSS J0248+0009 ($z = 1.64$, $\Delta\theta = 6\farcs8$, $R = 41.9\ h^{-1}$ kpc). [*See the electronic edition of the Journal for a color version of this figure.*]

indicate the redshift limits $0.7 \leq z \leq 3.0$ of the sample, and the symbols and dotted and short-dashed curves are the same as in Figure 3.

6. CLUSTERING ANALYSIS

A measurement of quasar clustering on the small scales probed by our binary sample, $10\ h^{-1}$ kpc $\lesssim R_{\rm prop} \lesssim 1\ h^{-1}$ Mpc, is unprecedented. Our strategy has been to overcome the fiber collision limitation and high level of shot noise by following up close pairs of quasars to magnitudes $i < 21$, fainter than the flux limit of the quasar SDSS.

As our pairs have a fainter flux limit than the underlying parent quasar catalog, and the mean density at this limit cannot be determined from the brighter sample, we cannot use the conventional technique of Monte Carlo integration of a random catalog to compute the correlation function. However, the mean number density of quasars as a function of magnitude and redshift is well known (Croom et al. 2004b; Richards et al. 2005) and can be computed from the quasar luminosity function. Below, we explain how we model the quasar luminosity function. We then introduce an estimator for the quasar correlation function that takes the incompleteness of our pair survey into account. After determining the selection function of our clustering subsample, we compute its correlation function and compare it to previous clustering measurements extrapolated down to the scales $R_{\rm prop} \lesssim 1\ h^{-1}$ Mpc probed by our binaries.

6.1. *Modeling the Luminosity Function*

At low redshift $z < 2.3$, the quasar luminosity function has been measured by several groups (Boyle et al. 2000; Croom et al.

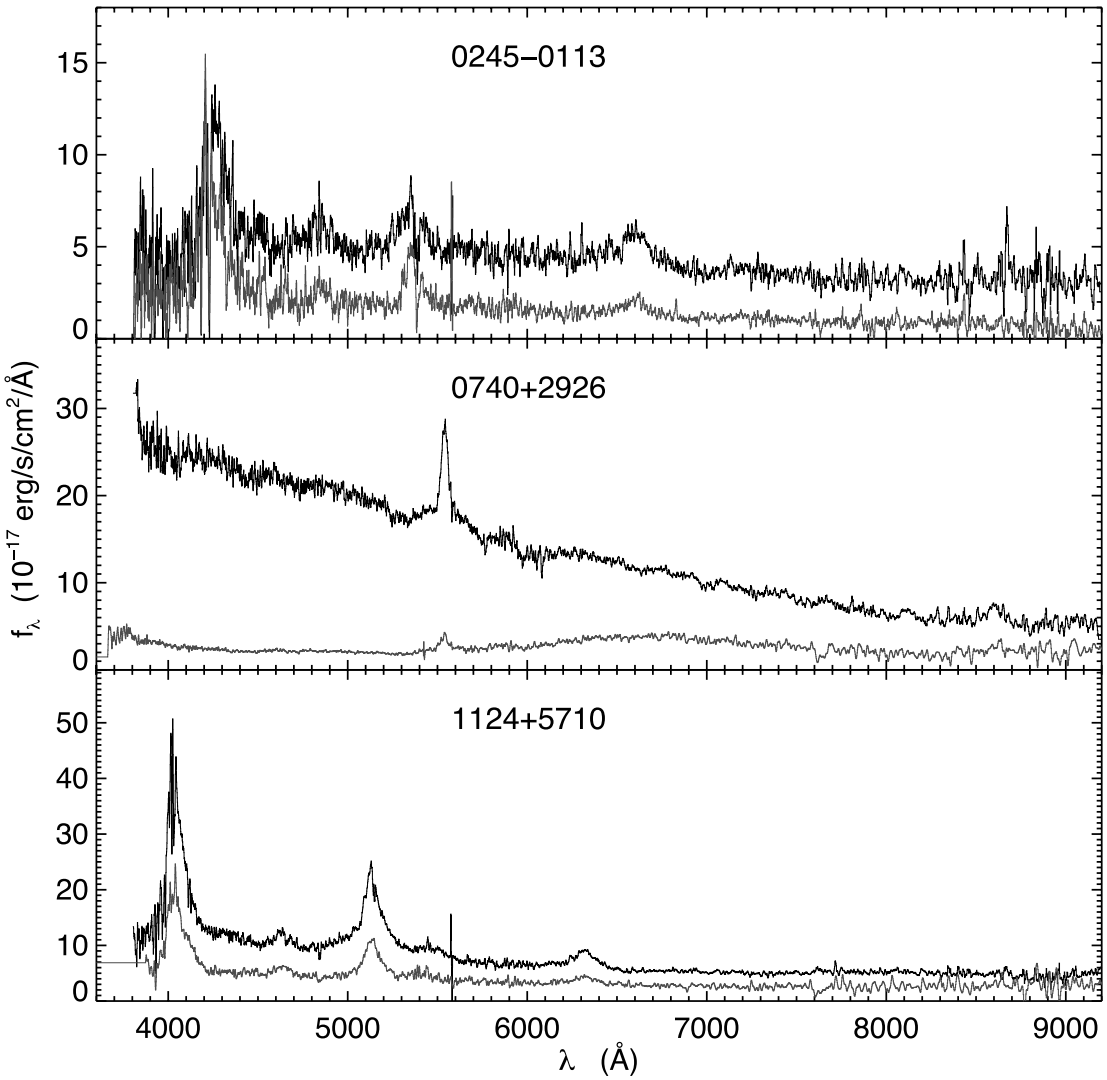

FIG. 6.—SDSS and APO spectra of both members of three binary quasars. The top panel shows the binary SDSS J0245−0113 ($z = 2.46$, $\Delta\theta = 4''.5$, $R_{\rm prop} = 26.3\ h^{-1}$ kpc), the middle panel shows SDSS J0740+2926 ($z = 0.98$, $\Delta\theta = 2''.6$, $R_{\rm prop} = 15.0\ h^{-1}$ kpc), and the bottom panel shows SDSS J1124+5710 ($z = 2.31$, $\Delta\theta = 2''.2$, $R_{\rm prop} = 12.7\ h^{-1}$ kpc). The binary in the top panel was a member of our overlap sample; hence, both quasars have SDSS spectra. For both the middle and bottom panels, the black curves are SDSS spectra of the brighter quasar in the pair, and the light curves are the APO spectra of the fainter companions. The absorption feature at 7600 Å in the lower two spectra is telluric. Although all three of these binaries have separations $\Delta\theta \lesssim 5''$ characteristic of gravitational lenses, deep optical and near-IR imaging show no lenses in the foreground. [*See the electronic edition of the Journal for a color version of this figure.*]

2004a; Richards et al. 2005). We use the double–power law B-band luminosity function (Boyle et al. 2000)

$$\Phi(M_B, z) = \frac{\Phi_*}{10^{0.4(\beta_l+1)\left[M_B - M_B^*(z)\right]} + 10^{0.4(\beta_h+1)\left[M_B - M_B^*(z)\right]}}, \qquad (5)$$

where $\beta_l = -1.58$, $\beta_h = -3.41$, and $\Phi_* = 360(h/0.50)^3$ Gpc^{-3} mag^{-1}, which is in good agreement with the recent measurement of Richards et al. (2005) to fainter magnitudes. The evolution of the break luminosity $M_B^*(z)$ follows

$$M_B^* = M_B^*(0) - 2.5(k_1 z + k_2 z^2), \qquad (6)$$

with $k_1 = 1.36$, $k_2 = -0.27$, and $M_B^*(0) = -21.15 + 5\log h$. The quasar luminosity function is poorly constrained for redshifts $2.6 \le z \le 2.9$, because quasar colors cross the stellar locus (see, e.g., Richards et al. 2001a) in this range and color-selected samples suffer high incompleteness. As we desire to predict the number density of quasars in the redshift range $0.7 < z < 3.0$ probed by our clustering subsample, we devise a simple interpolation scheme to cover the range $2.3 < z < 3.0$: Wyithe & Loeb (2002a) used a simple analytical model to fit the double–power law luminosity function in equation (5) to both the Fan et al. (2001) high-redshift ($z > 3.6$) luminosity function and the Boyle et al. (2000) low-redshift ($z < 2.3$) luminosity function. For redshifts $z < 2.3$ we use the Boyle et al. (2000) expression in equation (5). In the range $2.3 < z < 3.0$ we simply linearly interpolate between equation (5) and the Wyithe & Loeb (2002a) fit. Since the number of binary quasars in our clustering sample in this redshift range is relatively small, our conclusions are insensitive to any uncertainties in this procedure.

Although the luminosity functions we are considering are expressed in terms of M_B, both the spectroscopic SDSS and our binary quasar survey have flux limits in the i band. Thus, in order to compute the number of quasars above our flux limit, we need to know the cross-filter K-correction, $K_{Bi}(z)$, between

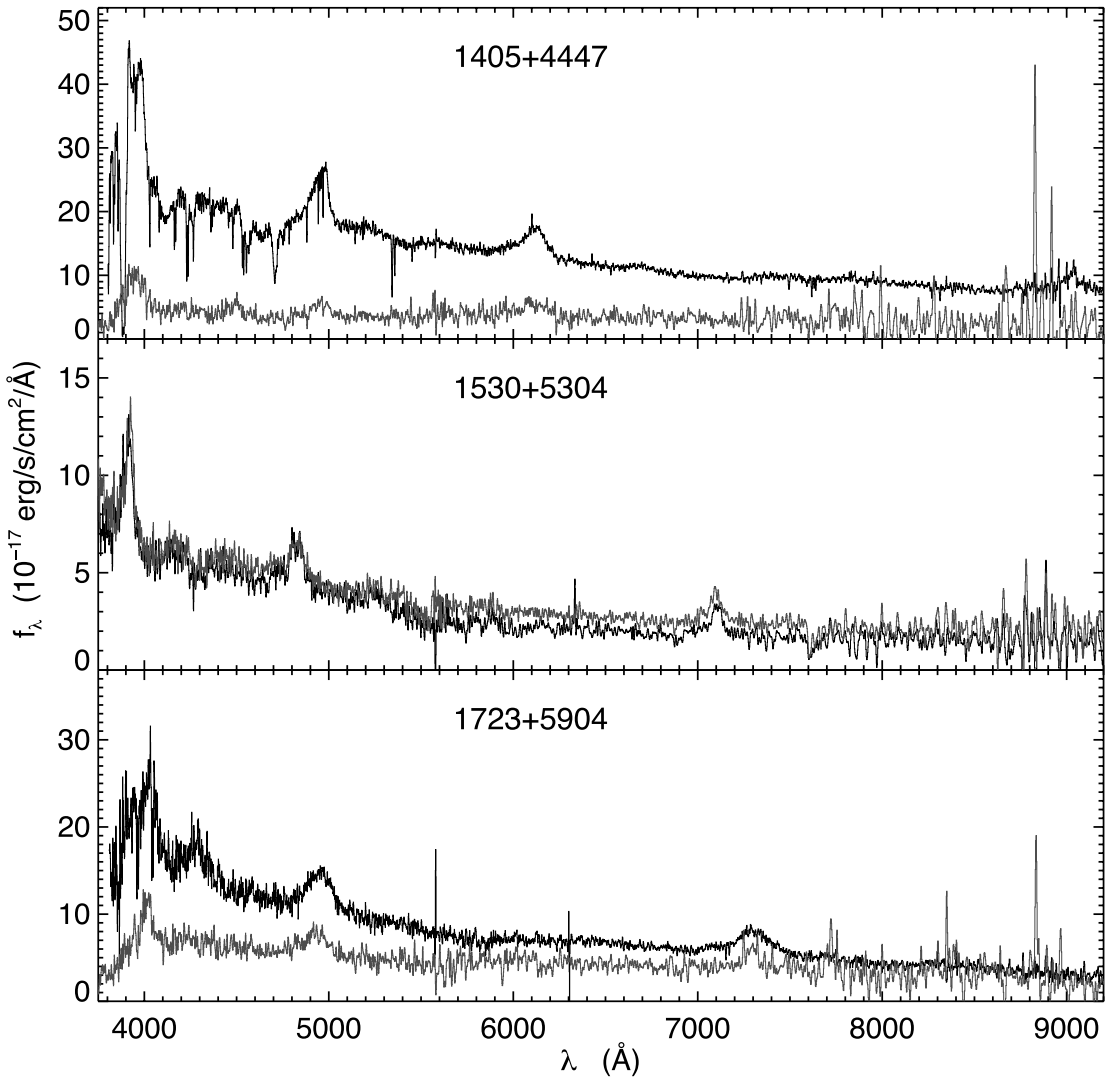

FIG. 7.—SDSS and APO spectra of both members of three binary quasars. The top panel shows the binary SDSS J1405+4447 ($z = 2.23$, $\Delta\theta = 7''.4$, $R = 142.8\ h^{-1}$ kpc), the middle panel shows SDSS J1530+5304 ($z = 1.53$, $\Delta\theta = 4''.1$, $R = 63.3\ h^{-1}$ kpc), and the bottom panel shows SDSS J1723+5904 ($z = 1.60$, $\Delta\theta = 3''.7$, $R = 59.0\ h^{-1}$ kpc). The binary in the middle panel is a member of the photometric sample, and both spectra were taken at APO. In the other two panels, the black curves are SDSS spectra of the brighter quasar in the pair, and the light curves are the APO spectra of the fainter companion. Deep imaging of SDSS J1405+4447 and SDSS J1723+5904 shows no lens in the foreground. The absorption features at 7600 Å are telluric. [*See the electronic edition of the Journal for a color version of this figure.*]

apparent magnitude i and absolute magnitude B (see, e.g., Hogg et al. 2002):

$$M_B = i - DM(z) - K_{Bi}(z), \tag{7}$$

where $DM(z)$ is the distance modulus. We compute $K_{Bi}(z)$ from the SDSS composite quasar spectrum of Vanden Berk et al. (2001) and the Johnson B and SDSS i filter curves.

The number density of quasars brighter than the flux limit i' is an integral over the luminosity function,

$$n(z,\ i < i') = \int_{M_B^{\rm bright}}^{M_B^{i'}} dM_B\, \Phi(M_B,\ z), \tag{8}$$

where $M_B^{\rm bright}(z)$ and $M_B^{i'}(z)$ are the absolute magnitudes corresponding to the bright- and faint-end apparent magnitude limits as per equation (7).

To check our model, we compute the cumulative number magnitude counts $n(<i)$ for the redshift range $0.3 < z < 3.0$ and compare to the measurement over the same redshift interval by Vanden Berk et al. (2005). We find that our model slightly overestimates the number counts of quasars. Specifically, Vanden Berk et al. (2005) measured $n(<18.5) = 3.74\ \deg^{-2}$, whereas our model predicts $n(<18.5) = 4.63\ \deg^{-2}$. We thus scale our model luminosity function down by this ratio so as to give the correct number counts for $i < 18.5$.

6.2. *Estimating the Correlation Function*

If it is true that quasars depart from the gravitational clustering hierarchy because of dissipative encounters, this would be expected to occur for separations smaller than some length scale characteristic of tidal effects or mergers. Proper rather than comoving coordinates are appropriate for such an investigation. However, clustering measurements are typically carried out in comoving coordinates, as these are most intuitive in the linear regime where objects are still moving with the Hubble flow. We compute the correlation function in both proper and comoving units, but for definiteness we use comoving units in the equations that follow.

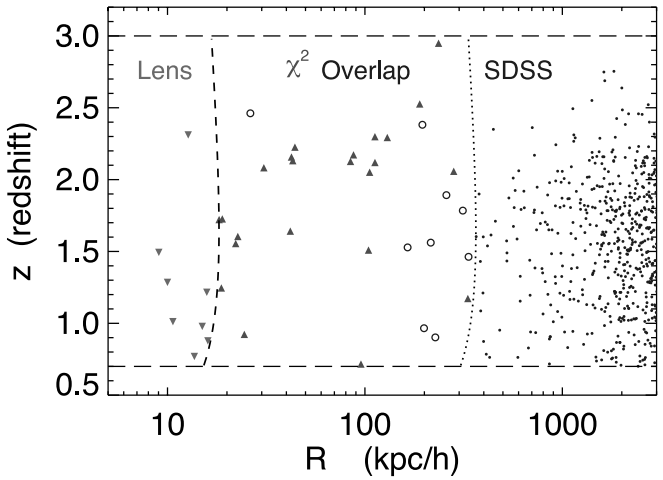

FIG. 8.—Range of redshifts and proper transverse separations probed by the binary quasars in our clustering subsample. The dots show binary quasars identified in the SDSS spectroscopic sample ($\theta > 60''$). The dotted line indicates the transverse separation corresponding to $\theta = 60''$. The open circles indicate pairs from the overlapping plates. These pairs are required to also meet the χ^2 selection criteria (eq. [4]). The upside-down and upright triangles show members of the lens and χ^2 samples, respectively. The short-dashed curve indicates the transverse separation corresponding to $\theta = 3''$, below which binaries are found with our lens algorithm. The horizontal long-dashed curves at $z = 0.7$ and 3.0 indicate the redshift limits of the clustering subsample. [*See the electronic edition of the Journal for a color version of this figure.*]

We consider quasars with a maximum velocity difference of $|\Delta v| < 2000$ km s^{-1}; thus, we measure the redshift space correlation function projected over this velocity interval:

$$w_p(R,\ z) = \int_{-v_{\max}/aH(z)}^{v_{\max}/aH(z)} \xi_s(R,\ s,\ z)\, ds, \tag{9}$$

where ξ_s is the quasar correlation function in redshift space, $v_{\max} = 2000$ km s^{-1}, $H(z)$ is the expansion rate at redshift z, and the factor of $a = 1/(1+z)$ converts the redshift distance to comoving units.

The redshift space correlation function $\xi_s(R, s, z)$ is the convolution of the velocity distribution in the redshift direction, $F_v(v_z)$, with the real space correlation function $\xi(r, z)$:

$$\xi_s(R,\ s,\ z) = \int_{-\infty}^{\infty} \xi\left(\sqrt{R^2 + x^2},\ z\right) f_v(H(z)(x - s))\, dx. \tag{10}$$

The radial velocity distribution $F_v(v_z)$ has contributions from both peculiar velocities and uncertainties in the systemic redshifts of the quasars. Provided that the distance in redshift space over which we project contains most of the area under F_v, it is a good approximation to replace the redshift space correlation function ξ_s under the integral in equation (9) with the real space correlation function ξ, since radial velocities will simply move pairs of points within the volume.

The small number of close pairs will limit the number of bins in R for which we can measure the correlation function. Since w_p may change significantly over these large bins, we choose to measure the volume-averaged projected correlation function integrated over each radial bin. We denote this dimensionless quantity by $\bar{W}_p$. Within a comoving bin $[R_{\min}, R_{\max}]$ it can be written as

$$\bar{W}_p(R_{\min},\ R_{\max},\ z)\, \frac{\int_{-v_{\max}/aH(z)}^{v_{\max}/aH(z)} \int_{R_{\min}}^{R_{\max}} \xi(R,\ s,\ z) 2\pi R\, dR\, ds}{V_{\rm shell}}, \tag{11}$$

where $V_{\rm shell}$ is the volume of the cylindrical shell in redshift space:

$$V_{\rm shell} = \pi\left(R_{\max}^2 - R_{\min}^2\right)\left[\frac{2v_{\max}}{aH(z)}\right]. \tag{12}$$

The correlation function of a point process is computed by comparing the number of pairs detected to the number expected in the absence of clustering, taking into account the sample limits. We choose the estimator

$$1 + \bar{W}_p(R_{\min},\ R_{\max}) = \frac{\langle QQ\rangle}{\langle QR\rangle}. \tag{13}$$

Usually, random catalogs are constructed to determine the average number of data-random pairs $\langle QR\rangle$. However, a subtlety arises in the current context, because for $\Delta\theta < 60''$ we have targeted the companion quasars (i.e., the quasars discovered from follow-up observations) to fainter magnitudes than the quasars from the parent spectroscopic sample. Rather than estimate the correlation function from the number of pairs, we use the number of *companions*. Specifically, $\langle QQ\rangle$ is defined to be the number of companions about quasars in the parent sample in a given comoving transverse radial bin $[R_{\min}, R_{\max}]$, and $\langle QR\rangle$ is the average number of random companions in this radial bin in the absence of clustering. In the case in which the parent and companion samples are distinct (as is the case for the lens and χ^2 samples), then $\langle QQ\rangle$ is just the number of binaries in the bin in question. However, if the parent and companion samples are identical (as is the case for the overlap and spectroscopic samples), then $\langle QQ\rangle$ is *twice* the number of pairs, since each of the two quasars in the parent sample has a companion.

Our model of the luminosity function in § 6.1 is used to compute the average number of random companions R about the quasars Q in each parent quasar sample, taking into account the flux limits and various sources of incompleteness. We separately compute the quasar-random contribution for each selection algorithm used to define our clustering sample, and we then add the results. Specifically, for a comoving transverse radial bin $[R_{\min}, R_{\max}]$ centered on R, we can write

$$\langle QR\rangle = \sum_j^{N_{\rm QSO}} n\left(z_j,\ i < i'\right) V_{\rm shell}\, S\left(z_j,\ \theta_j\right), \tag{14}$$

where $n(z_j,\ i < i')$ is the number density of quasars above the flux limit i', $V_{\rm shell}$ is the volume of each bin in equation (12), and the sum is over all quasars in the parent sample. The quantity $S(z_j, \theta_j)$ is the selection probability of detecting a companion about the jth quasar. It is a function of angle and redshift, since these quantities parameterize our various selection algorithms, as discussed in § 3. Here $\theta_j = R/D(z)$ is the angle onto which the (logarithmic) center of the bin projects for a quasar at redshift z, and $D(z)$ is the comoving distance.

In what follows we compare our measured correlation function to previous larger scale (1–30 h^{-1} Mpc) clustering measurements extrapolated as a power law down to the scales probed by our binaries. Since $\bar{W}_p$ in equation (11) is a function of redshift, we must average it over the redshift distribution of our quasar sample before a comparison can be made to the measurement from equation (13),

$$\bar{W}_p(R_{\min},\ R_{\max}) = \frac{1}{N_{\rm QSO}} \sum_j^{N_{\rm QSO}} \bar{W}_p\left(R_{\min},\ R_{\max},\ z_j\right). \tag{15}$$

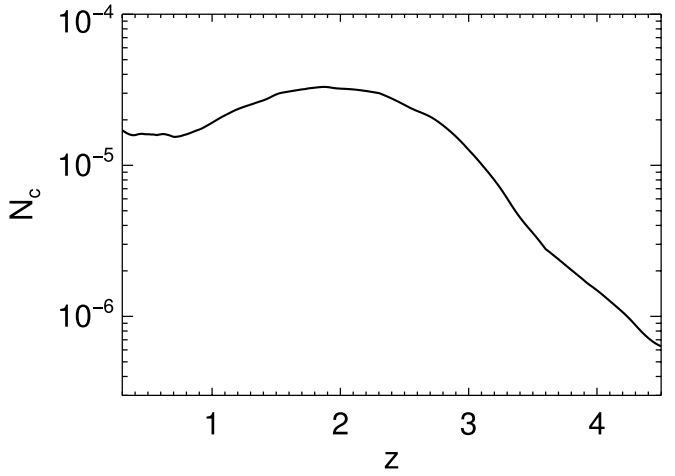

FIG. 9.—Expected mean number of companions per quasar with proper transverse separation 5 h^{-1} kpc $< R_{\rm prop} <$ 50 h^{-1} kpc and velocity difference $|\Delta v| <$ 2000 km s^{-1}, as a function of redshift calculated from eq. [16], which assumes that the large-scale quasar correlation function can be extrapolated as a power law to small scales. We used the correlation function parameters $\gamma = 1.53$ and $r_0 = 4.8\ h^{-1}$ Mpc measured by PMN04 from the 2dF quasar survey. A perfect survey, with no sources of incompleteness, is assumed. In a sample of ~50,000 quasars, the predicted number of binaries with 5 h^{-1} kpc $< R <$ 50 h^{-1} kpc is ~1. However, our clustering sample already contains 20 quasars with transverse separations this small, which is compelling evidence for excess clustering over what is expected from extrapolating the correlation function.

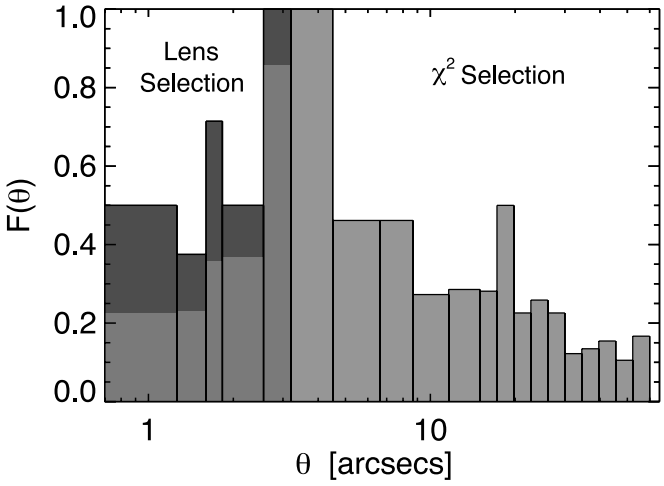

FIG. 10.—Angular selection function of binary quasars with $\theta < 60''$. We have pasted $F_{\rm lens}(\theta)$ and $F_{\chi^2}(\theta)$ together at $\theta = 3''$. For $\theta \leq 3''$, the dark and light histograms represent the upper and lower limits on the fraction of lens pair candidates observed to date, respectively. The histogram for $\theta > 3''$ shows the fraction of χ^2 pair candidates observed so far. [*See the electronic edition of the Journal for a color version of this figure.*]

In Figure 9 we show the prediction for the number of companions in the bin 5 h^{-1} kpc $< R_{\rm prop} <$ 50 h^{-1} kpc with $|\Delta v| <$ 2000 km s^{-1} as a function of redshift:

$$N_c = n(z,\ i < 21) V_{\rm shell}\left[1 + \bar{W}_p(5,\ 50,\ z)\right]. \qquad (16)$$

For only this figure, we ignore the redshift evolution of the correlation length and set $r_0 = 4.8\ h^{-1}$ Mpc. The expected mean number of companions per quasar with 5 h^{-1} kpc $< R <$ 50 h^{-1} kpc is ~2–3 $\times 10^{-5}$, so that for a *perfect* pair survey of ~50,000 quasars, we expect to find roughly one quasar pair in this interval. However, our clustering sample already contains 20 quasars with transverse separations this small. Although our pair survey is far from complete, there is already evidence for excess clustering over what is expected from extrapolating the correlation function power law. In the next two sections we make this argument more precise.

6.3. *Computing the Selection Function*

To estimate the correlation function, we compute the total number of random pairs expected from equation (14) by summing over the redshifts of the quasars in each parent sample around which we searched for candidate companions. However, we must first consider several sources of incompleteness. For the χ^2-selected sample, our $\chi^2 < 20$ cut results in the completeness fraction $C(z,\ \chi^2 < 20)$ shown in Figure 2. In addition, only a fraction of the pair candidates that satisfy the criteria for our lens and χ^2 selection algorithms have been observed to date, and the fraction of candidates observed varies with angular separation because of our tendency to observe small-separation pairs first. Finally, for the $\theta > 60''$ pairs that we find in the SDSS spectroscopic sample, the completeness fraction is just that of the quasar SDSS and does not vary with angle. The selection probability in equation (14) can therefore be written as

$$S(z,\ \theta) = \begin{cases} F_{\rm lens}(\theta), & \theta \leq 3'', \\ F_{\chi^2}(\theta) C(z|\chi^2 < 20), & 3'' < \theta \leq 60'', \\ F_{\rm spec}, & \theta > 60'', \end{cases} \qquad (17)$$

where $F_{\rm lens}(\theta)$, $F_{\chi^2}(\theta)$, and $F_{\rm spec}$ are the completeness fractions of the lens, χ^2, and spectroscopic samples, respectively.

We take $F_{\rm spec} = 0.95$ following Vanden Berk et al. (2005). The angular selection functions, $F_{\rm lens}(\theta)$ and $F_{\chi^2}(\theta)$, of the lens and χ^2 selection algorithms are computed by comparing, in bins, the number of pair candidates that have been observed to date to the total number of candidates.

For $\theta < 15''$ we choose the bin spacing such that each bin contains at least six objects. For $15'' < \theta < 60''$ we use 10 logarithmically spaced angular bins. The selection probability for the angular bin $[\theta_k, \theta_{k+1}]$ is

$$F_k = \frac{N_{\rm obs}}{N_{\rm obs} + N_{\rm rem}}, \qquad (18)$$

where $N_{\rm obs}$ is the number of objects observed and $N_{\rm rem}$ is the number of objects remaining. There is an uncertainty in the number of remaining candidates for the lens selection, which is based on the goodness of fit of a multicomponent PSF to the images of SDSS quasars (Pindor et al. 2003; Inada et al. 2003a). Because our observations were heavily biased toward those candidates that were likely to be quasar pairs, we bracket the angular selection function $F_{\rm lens}(\theta)$ with upper and lower limits corresponding to pessimistic and optimistic assessments of the number of remaining candidates that are likely to be confirmed as binaries. The lens candidates are given a grade of A, B, or C determined by the goodness of fit of the multicomponent PSF. For the lower limit on $F_{\rm lens}(\theta)$, $N_{\rm rem}$ is taken to be all candidates, whereas for the upper limit $N_{\rm rem}$ is restricted to only the candidates that received a grade of A. Note that to be conservative, we ignore the intrinsic incompleteness of the lens selection algorithm, which is a function of separation, magnitude, and flux ratio (Pindor et al.

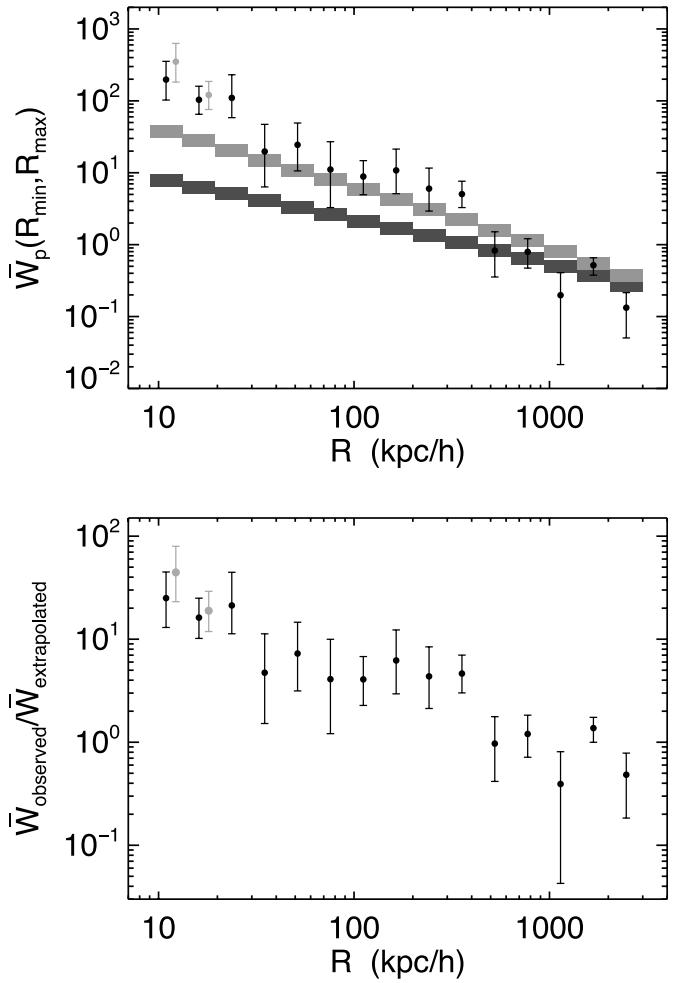

FIG. 11.—Small-scale quasar clustering in proper coordinates. *Top*: Comparison of the projected correlation function $\bar{W}_p(R_{\rm min}, R_{\rm max}, z)$ (see eq. [11]) measured from our clustering sample with the prediction of the large-scale measurement of PMN04, extrapolated as a power law down to the scales probed by our binaries. Error bars are 1 σ Poisson counting errors. The light circles show the measurement of the projected correlation function if we use the lower limit (optimistic) for the selection function of our lens algorithm (Fig. 10, *light histogram for* $\theta \leq 3''$) to predict the number of quasar-random pairs, rather than the upper limit, which is shown by the black circles. The light circles are offset slightly to the right for the sake of illustration. Dark and light rectangles indicate the predictions based on the large-scale measurements of PMN04 for $\gamma = 1.53$ and 1.8, respectively, where the heights of the rectangles indicate the range of predictions based on 1 σ errors in the correlation length measurements, and the widths indicate the bin used for each measurement. *Bottom*: Ratio of the projected correlation function to the (best-fit $\gamma = 1.53$) prediction of PMN04. [*See the electronic edition of the Journal for a color version of this figure.*]

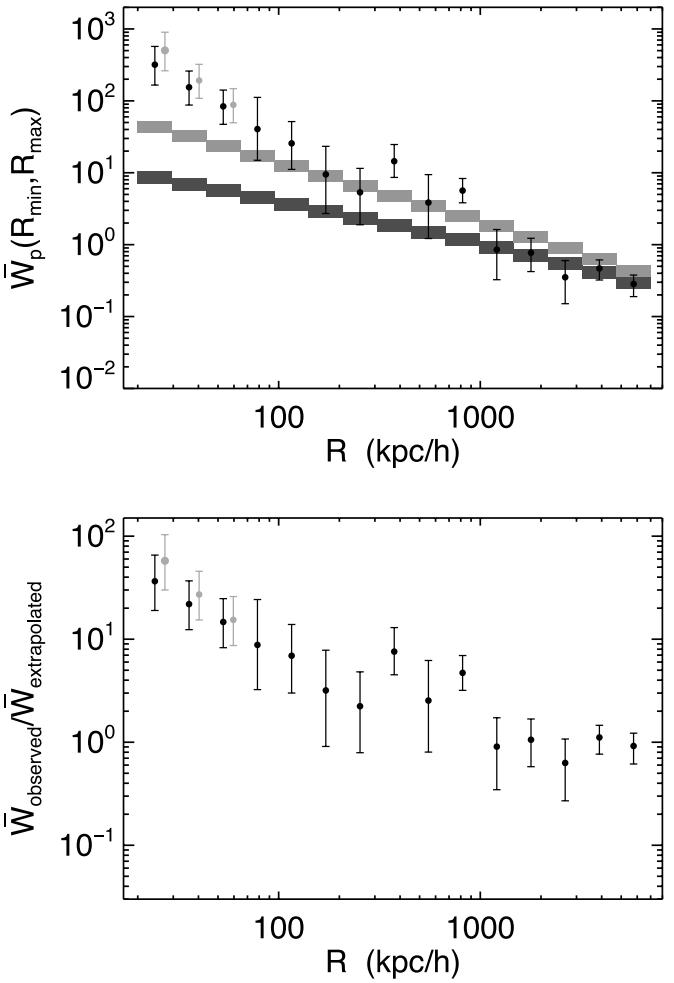

FIG. 12.—Same as Fig. 11, but in comoving units. [*See the electronic edition of the Journal for a color version of this figure.*]

2003) of the pair, and focus only on the incompleteness of our observations of the candidates.

The color-color diagrams of the candidates identified by χ^2 selection were visually inspected prior to observations, and those whose colors overlapped the stellar locus were given a lower priority. However, some interlopers were observed depending on a variety of criteria. For instance, we were more likely to observe pairs with particularly small angular separations, redshifts $z > 2$ (because of their use for Lyα forest studies), or particularly bright magnitudes. Including the stellar locus interlopers identified by the χ^2 statistic as part of $N_{\rm rem}$ in equation (18) would overestimate the number of candidates likely to be quasar pairs and hence underestimate our selection function. To this end, we apply additional criteria to these remaining candidates to filter out color matches that are likely to be quasar-star pairs. However, all quasar-star pairs we confirmed spectroscopically are included as part of $N_{\rm obs}$ in equation (18). In this way, we conservatively err on the side of overestimating our selection completeness, or underestimating the correlation function.

In addition to using the criteria in equation (4), we only include χ^2 candidates that either (1) have colors consistent with the UV-excess region of color space ($u - g < 0.6$) but outside the region populated by white dwarfs (Richards et al. 2002b), (2) match a member of the faint photometric catalog of Richards et al. (2004) (extended to the DR3 region), or (3) are optically unresolved and match a FIRST radio source. Objects that satisfy these criteria have a $\gtrsim$90% probability of being a quasar. For the UV-excess criteria, we conservatively require that the candidates' 1 σ photometric errors leave them inside the UV-excess region and outside the white dwarf region. The angular selection function of our binary quasar survey is shown in Figure 10.

6.4. *Excess Clustering*

The individual quasar-random contributions for each selection algorithm were computed by carrying out the sum in equation (14) over the respective parent samples. Specifically, we summed over the 39,142 quasars that were the parent sample for the lens sample, the 59,608 (SDSS + 2QZ quasars) that were the parent sample of the χ^2 algorithm, and the 52,279 (SDSS only) quasars that made up the parent sample of the spectroscopic sample.

For the proper (comoving) projected correlation functions, we binned our clustering sample into 15 logarithmically spaced bins in

TABLE 6
PROJECTED CORRELATION FUNCTION IN PROPER COORDINATES

$R_{\rm min}$	$R_{\rm max}$	$\langle QQ\rangle$	$\langle QR\rangle$	$\langle QR\rangle_{\rm perfect}$	$\bar{W}_p$	$\bar{W}_p^{\rm PMN}$	Ratio
9.00	13.26	4	0.02014 (0.01136)	0.03147	197.60 (350.98)	7.89	25.0 (44.5)
13.26	19.53	7	0.06694 (0.05749)	0.06922	103.57 (120.76)	6.40	16.2 (18.9)
19.53	28.76	5	0.04506	0.2240	109.96	5.17	21.3
28.76	42.37	2	0.09635	0.4860	19.76	4.18	4.73
42.37	62.40	3	0.11784	1.055	24.46	3.37	7.26
62.40	91.92	2	0.1654	2.288	11.09	2.71	4.09
91.92	135.39	6	0.6090	4.964	8.85	2.17	4.07
135.39	199.42	7	0.5938	10.77	10.79	1.74	6.22
199.42	293.74	8	1.142	23.37	6.01	1.38	4.36
293.74	432.67	20	3.305	37.30	5.05	1.09	4.64
432.67	637.31	23	12.59	13.25	0.83	0.85	0.97
637.31	938.74	49	27.31	28.75	0.79	0.66	1.20
938.74	1382.73	71	59.26	62.38	0.20	0.50	0.39
1382.73	2036.71	195	128.6	135.3	0.52	0.38	1.37
2036.71	3000.00	316	279.0	293.6	0.13	0.27	0.48

NOTES.—Given are the data for the clustering measurements shown in Fig. 11. The 15 logarithmically spaced bins of proper transverse separation are given by $R_{\rm min}$ and $R_{\rm max}$ in h^{-1} kpc. The number of observed pairs in our clustering subsample for each bin is given by $\langle QQ\rangle$. Our calculation of the number of random pairs in each bin is $\langle QR\rangle$ (eq. [14]), and $\langle QR\rangle_{\rm perfect}$ is the expected number of random pairs for a "perfect" survey with no sources of incompleteness. Our measurement of the projected correlation function is given by $\bar{W}_p(R_{\rm min},\ R_{\rm max})$. The quantity $\bar{W}_p^{\rm PMN}(R_{\rm min},\ R_{\rm max})$ is the prediction from the larger scale clustering measurements of PMN04 ($\gamma = 1.53$), extrapolated as a power law down to the scale probed by our binaries and averaged over the redshift distribution of our parent quasar sample (see eq. [15]). The ratio of our measurement to the prediction from PMN04 ($\gamma = 1.53$) is given in the last column. The quantities in parentheses are the measurements if we use the lower limit for the selection function of the lens algorithm (Fig. 10, *light histogram for* $\theta \leq 3''$) to predict $\langle QR\rangle$, which corresponds to the light circles in Fig. 11.

the range 9 h^{-1} kpc $< R_{\rm prop} <$ 3 h^{-1} Mpc (20 h^{-1} kpc $< R <$ 7 h^{-1} Mpc), which are shown in the top panels of Figures 11 and 12. The error bars are 1 σ Poisson counting errors, where we used the fitting formula in Gehrels (1986) for $N < 30$. The light circles show the measurement of the projected correlation function if we use the lower limit (optimistic) for the selection function of our lens algorithm (Fig. 10, *light histogram for* $\theta \leq 3''$) to predict the number of quasar-random pairs, while the black circles use the upper limit. Uncertainty in our selection function changes only the innermost few bins, because our lens algorithm is restricted to angular separations $\theta < 3''$. These light circles are offset slightly to the right for the sake of illustration.

These projected correlation functions are compared to an extrapolation of the large-scale power laws measured by PMN04, which are indicated by the dark and light rectangles.[21] Taking all redshifts together, PMN04 measured a best-fit slope of $\gamma = 1.53$

[21] The PMN04 correlation function is in comoving coordinates. For the proper correlation function, we translated the correlation lengths to proper coordinates in each element of the average in eq. (15).

TABLE 7
PROJECTED CORRELATION FUNCTION IN COMOVING COORDINATES

$R_{\rm min}$	$R_{\rm max}$	$\langle QQ\rangle$	$\langle QR\rangle$	$\langle QR\rangle_{\rm perfect}$	$\bar{W}_p$	$\bar{W}_p^{\rm PMN}$	Ratio
20.00	29.56	4	0.01251 (0.007935)	0.02452	318.69 (503.12)	8.73	36.5 (57.6)
29.56	43.68	5	0.03213 (0.02595)	0.06007	154.61 (191.66)	7.06	21.9 (27.1)
43.68	64.54	5	0.05895 (0.05623)	0.1674	83.81 (87.92)	5.71	14.7 (15.4)
64.54	95.38	3	0.07226	0.3886	40.52	4.61	8.80
95.38	140.95	3	0.1127	0.8487	25.63	3.71	6.91
140.95	208.28	2	0.1907	1.853	9.49	2.98	3.18
208.28	307.80	3	0.4731	4.047	5.34	2.39	2.24
307.80	454.85	10	0.6467	8.839	14.46	1.91	7.58
454.85	672.16	5	1.032	18.75	3.85	1.52	2.54
672.16	993.29	21	3.160	29.00	5.65	1.20	4.71
993.29	1467.84	20	10.80	13.29	0.85	0.94	0.91
1467.84	2169.12	42	23.71	24.96	0.77	0.73	1.06
2169.12	3205.45	70	51.78	54.51	0.35	0.56	0.63
3205.45	4736.89	166	113.1	119.0	0.47	0.42	1.11
4736.89	7000.00	317	246.9	259.9	0.28	0.31	0.92

NOTES.—Given are the data for the clustering measurements shown in Fig. 12. The 15 logarithmically spaced bins of proper transverse separation are given by $R_{\rm min}$ and $R_{\rm max}$ in h^{-1} kpc. The number of observed pairs in our clustering subsample for each bin is given by $\langle QQ\rangle$. Our calculation of the number of random pairs in each bin is $\langle QR\rangle$ (eq. [14]), and $\langle QR\rangle_{\rm perfect}$ is the expected number of random pairs for a "perfect" survey with no sources of incompleteness. Our measurement of the projected correlation function is given by $\bar{W}_p(R_{\rm min},\ R_{\rm max})$. The quantity $\bar{W}_p^{\rm PMN}(R_{\rm min},\ R_{\rm max})$ is the prediction from the larger scale clustering measurements of PMN04 ($\gamma = 1.53$), extrapolated as a power law down to the scale probed by our binaries and averaged over the redshift distribution of our parent quasar sample (see eq. [15]). The ratio of our measurement to the prediction from PMN04 ($\gamma = 1.53$) is given in the last column. The quantities in parentheses are the measurements if we use the lower limit for the selection function of the lens algorithm (Fig. 10, *light histogram for* $\theta \leq 3''$) to predict $\langle QR\rangle$, which corresponds to the light circles in Fig. 12.

and $r_0 = 4.8\ h^{-1}$ Mpc, consistent with the measurement by Croom et al. (2001, 2005). They also detected evolution of the correlation length r_0 with look-back time by splitting the sample into three redshift bins ($0.8 < z < 1.3$, $1.3 < z < 1.7$, and $1.7 < z < 2.1$). As there is significant covariance between the slope and amplitude, they quoted correlation lengths (and errors) in these bins at two slopes: the best-fit value $\gamma = 1.53$ and a steeper value of $\gamma = 1.8$. The dark rectangles indicate the prediction for the projected correlation function based on an extrapolation of the $\gamma = 1.53$ large-scale power law, whereas the light rectangles are for $\gamma = 1.8$. The heights of the rectangles are the range of predictions based on the 1 σ errors on the correlation lengths (for each redshift interval) published by PMN04, and the widths of the rectangles indicate the bin used for each measurement. Note that we include the evolution of the correlation length (from the values of Table 2 in PMN04) in the average in equation (15). The ratios of the measured projected correlation functions to the extrapolation of the best-fit $\gamma = 1.53$ predictions of PMN04 are shown in the bottom panels of Figures 11 and 12.

A summary of the data plotted in these figures is given in Tables 6 and 7. In the tables we compare our calculation for the number of random pairs in each bin $\langle QR \rangle$ (eq. [14]) for our survey to $\langle QR \rangle_{\rm perfect}$, which is the expected number of random pairs for a "perfect" survey with no sources of incompleteness. A comparison of these two quantities is a measure of our incompleteness in each bin.

Our clustering measurement agrees with the measurements of PMN04 for large proper (comoving) separations $R_{\rm prop} \gtrsim 400\ h^{-1}$ kpc ($R \gtrsim 1\ h^{-1}$ Mpc), where the PMN04 measurements are valid. However, we detect a significant excess over the expectation from extrapolating the power law of the correlation function to smaller scales. The uncertainties are large because of shot noise, our uncertain selection function for $\theta < 3''$, and the range of permitted large-scale correlation function slopes. For the best-fit large-scale slope $\gamma = 1.53$, the excess is an order of magnitude for proper (comoving) separations $R_{\rm prop} \lesssim 40\ h^{-1}$ kpc ($R \lesssim 100\ h^{-1}$ kpc) and is largest ($\sim$30) on the smallest scales $R_{\rm prop} \sim 15\ h^{-1}$ kpc ($R \sim 30\ h^{-1}$ kpc). For the steeper slope $\gamma = 1.8$, the excess is smaller by a factor of 4–5.

Our clustering statistic $W_p(R_{\rm min}, R_{\rm max})$ is the average over a cylinder shell with velocity extent 4000 km s^{-1}, corresponding to a typical extent $r_{\rm prop} \sim 18\ h^{-1}$ Mpc ($r \sim 44\ h^{-1}$ Mpc). For a power-law correlation function $\xi(r) = (r/r_0)^{-\gamma}$, $W_p(R_{\rm min}, R_{\rm max})$ progressively flattens toward small scales, as is seen in the dark rectangles in the top panels of Figures 11 and 12. In contrast, our measured $W_p(R_{\rm min}, R_{\rm max})$ does not flatten but rather resembles a power law *in projection*. This necessarily implies that the true three-dimensional correlation function of quasars is not a power law $\xi(r)$ but rather gets *progressively steeper on small scales*.

7. DISCUSSION

On large proper comoving scales $\gtrsim 1\ h^{-1}$ Mpc, quasars at $z \sim 1.5$, similar to high-redshift galaxies, are strongly biased and have nearly the same correlation length that galaxies do in the local universe. In § 6 we argued that the correlation function of quasars becomes significantly *steeper* on submegaparsec scales. Does small-scale galaxy clustering (or quasar-galaxy clustering) show a similar trend? As we compare to previous clustering measurements in this section, all distances quoted are comoving.

At low redshift, Zehavi et al. (2004) measured the projected correlation function of the nearby ($z \lesssim 0.2$) SDSS main galaxy sample down to $\sim$100 h^{-1} kpc and found only small deviations from a power law $\gamma \sim -1.9$. At intermediate redshift ($0.2 \lesssim z \lesssim 0.3$), Masjedi et al. (2005) recently measured the small-scale clustering of the SDSS luminous red galaxies, using a novel statistical technique to overcome the incompleteness caused by fiber collisions. They found that the correlation function is surprisingly close to an r^{-2} power law over 5 orders of magnitude in comoving separation, down to scales as small as 10 h^{-1} kpc.

Another complementary set of low-redshift observations that probe clustering on small scales (10 h^{-1} kpc to 1 h^{-1} Mpc) is the SDSS galaxy-galaxy lensing studies (Guzik & Seljak 2002; Sheldon et al. 2004), which measure the galaxy–dark matter cross-correlation function. No excess small-scale clustering over a power law was detected in these studies either.

A comparison with small-scale galaxy clustering at high redshift is clearly more relevant to our purposes. Adelberger et al. (2003) and Coil et al. (2004) have measured the correlation function of galaxies at $z \sim 3$ and $z \sim 1$, respectively, down to scales as small as $\sim$100–200 h^{-1} kpc, and no small-scale excess clustering was found. As the redshift ranges of these measurements bracket the redshift range probed by our sample of binary quasars, we expect that galaxies in the redshift desert, $z \sim 1.4$–2.5, coeval with the bulk of our binary quasars (see Fig. 3), also will not show any enhancement in small-scale clustering.

Thus, as first suggested by Djorgovski (1991), quasars at $z \sim 1.5$ depart from the power-law clustering hierarchy followed by galaxies, both in the local universe and at high redshift. Galaxy interactions are often implicated as a means of triggering, fueling, or forming active galactic nuclei (AGNs; Toomre & Toomre 1972; Barnes & Hernquist 1996; Bahcall et al. 1997), and it has been claimed by several authors that excess quasar clustering is the hallmark of these dissipative interactions (Djorgovski 1991; Kochanek et al. 1999; Mortlock et al. 1999). However, if this is the case, a similar small-scale enhancement is to be expected in the quasar-galaxy correlation function, as follows.

If the quasar-quasar correlation function is ξ_{QQ} and quasars trace galaxy overdensities with a linear relative bias b_Q defined by $\delta_Q = b_Q \delta_G$, then the ratio of the quasar-quasar correlation to the galaxy-galaxy correlation is $\xi_{QQ}/\xi_{GG} = b_Q^2$, and the ratio of the quasar-galaxy cross-correlation function to galaxy-galaxy clustering is $\xi_{QG}/\xi_{GG} = b_Q$. Since we have argued that small-scale quasar clustering is enhanced relative to galaxy clustering at the same redshift, we expect to see the square root of that enhancement in the quasar-galaxy cross-correlation.

It has long been known that quasars are associated with enhancements in the distribution of galaxies (Bahcall et al. 1969; Yee & Green 1984, 1987; Bahcall & Chokshi 1991; Laurikainen & Salo 1995; Smith et al. 1995, 2000; Hall et al. 1998; Hall & Green 1998), and the foregoing argument has led us to ask if there is a small-scale excess of galaxy pairs around quasars.[22] However, nearly all studies of quasar-galaxy correlations have been restricted to low redshifts ($z \lesssim 0.6$) and therefore low luminosity. Recently, Adelberger & Steidel (2005) measured the cross-correlation of high-redshift ($1.8 \lesssim z \lesssim 3.5$) Lyman break galaxies (LBGs) with AGNs. A best-fit correlation length of $r_0 = 4.7\ h^{-1}$ Mpc (at a fixed slope of $\gamma = 1.6$) was measured for bright AGNs in the luminosity range considered here, which is very close to the autocorrelation length of LBGs (Adelberger et al. 2003). This measurement does not probe small scales because it was limited to quasar-galaxy pairs with separations $>60''$, corresponding to $\gtrsim 1\ h^{-1}$ Mpc. However, the small-scale

[22] We note that the disagreement in the literature on whether radio-loud quasars are located in richer environments (Yee & Green 1984, 1987; Ellingson et al. 1991) or not (Fisher et al. 1996; McLure & Dunlop 2001; Finn et al. 2001; Wold et al. 2001) is not an issue in the current context, since only one close binary in our clustering subsample, LBQS 1429−008, has a radio-loud member.

$<60''$ clustering of LBGs around quasars seems to be consistent with this result (K. Adelberger 2005, private communication). While it is puzzling that the quasar-LBG cross-correlation does not seem to show a small-scale enhancement, it is conceivable that fainter galaxies below the flux limit ($\mathcal{R}_{\rm AB} \leq 25.5$ or $\sim 0.4L_*$) of the LBG survey (Steidel et al. 2003) could still show a small-scale clustering excess.

Historically, there has been significant scatter in the low-redshift measurements of quasar-galaxy correlations (see Brown et al. 2001, Table 1, for a compilation of recent studies) caused by heterogeneous quasar samples, methodology, and imaging depths. Furthermore, the measurement of a factor of ~ 4 enhancement of the number of companion galaxies around quasars compared to the mean number around galaxies, measured by the *Hubble Space Telescope* studies of ~ 40 nearby AGNs by Fisher et al. (1996) and McLure & Dunlop (2001), has been called into question by Finn et al. (2001) as being the result of sample biases. We thus focus on the most recent determinations of quasar-galaxy correlations, albeit at low redshifts $z \lesssim 0.3$, by the 2dF survey and SDSS; these surveys have samples of $\sim 10{,}000$ AGNs surrounded by $\sim 100{,}000$ galaxies at their disposal.

Croom et al. (2004b) and Wake et al. (2004) measured the ratio $\xi_{QG}/\xi_{GG} = b_Q$, in the 2dF survey and SDSS, respectively, finding it to be consistent with unity on small and large scales. The Croom et al. (2004b) measurement extends down to $\sim 900\ h^{-1}$ kpc, whereas the Wake et al. (2004) measurement probes down to scales of $\sim 400\ h^{-1}$ kpc. Both of these studies cross-correlated spectroscopic samples of galaxies with spectroscopic samples of AGNs; hence, they are limited to low redshift $z \lesssim 0.3$, because the spectroscopic galaxy samples are shallow, and large scales, because of fiber collisions. At $z \sim 0.2$ the fiber collision limit corresponds to $\sim 160\ h^{-1}$ kpc in the SDSS and $\sim 80\ h^{-1}$ kpc in the 2dF. What is needed is a clustering study using photometric galaxies around spectroscopic quasars that could extend to redshift $z \sim 0.5$ and resolve the scales $R \sim 10\ h^{-1}$ kpc of most interest to us for the excess quasar clustering (see Serber et al. 2005).

8. SUMMARY AND CONCLUSIONS

We have presented a sample of 221 new quasar pairs with transverse separations $R_{\rm prop} < 1\ h^{-1}$ Mpc over the redshift range $0.5 \leq z \leq 3.0$. Of these, 65 have angular separations $\theta < 60''$ below the SDSS fiber collision scale. Our 26 new pairs with proper separations $R_{\rm prop} < 50\ h^{-1}$ kpc ($\theta < 10''$) more than double the number of binaries known with splittings this small. Although these binaries were discovered with a variety of selection algorithms, we defined a statistical subsample selected with homogeneous criteria and computed its selection function taking into account sources of incompleteness. We presented the first measurement of the quasar correlation function on the small proper (comoving) scales of 10–400 h^{-1} kpc (20 h^{-1} kpc to 1 h^{-1} Mpc). For a large-scale correlation function slope of $\gamma = 1.53$, we detect an order of magnitude excess clustering for proper (comoving) separations $R_{\rm prop} \lesssim 40\ h^{-1}$ kpc ($R \lesssim 100\ h^{-1}$ kpc), which grows to ~ 30 on the smallest scale probed by our sample, $R_{\rm prop} \sim 15\ h^{-1}$ kpc ($R \sim 30\ h^{-1}$ kpc). This excess is smaller by a factor of 4–5 if the large-scale correlation function has a steeper slope $\gamma = 1.8$.

We reviewed recent small-scale measurements of galaxy clustering and quasar-galaxy clustering and discussed the results in relation to the excess small-scale quasar clustering that we measured. The quasar-galaxy correlation function of redshift $z \sim 1.5$ quasars should show a small-scale clustering enhancement with amplitude roughly the square root of the enhancement detected here. However, existing studies of the environments of quasars at $z \sim 1.5$ have been plagued by small sample sizes and lack the statistics to address the clustering strength on the $\sim 100\ h^{-1}$ kpc scales of interest.

Deep imaging of the binaries published here will provide valuable information about their environments. The detection of significant overdensities of galaxies coeval with the binary would support the idea that enhanced quasar activity is triggered by galaxy interactions, and it might suggest that quasars at high redshift trace the biased peaks that are the progenitors of the rich clusters we see today (Efstathiou & Rees 1988; Cole & Kaiser 1989; Nusser & Silk 1993; Djorgovski et al. 1999, 2003; Djorgovski 1999). Intriguingly, Fukugita et al. (2004) took deep Subaru images of the $z = 4.25$ quasar discovered by Schneider et al. (2000) and found no evidence for an overdensity of galaxies. Similar deep imaging studies of high-redshift quasar environments (for single quasars) have been conducted by Infante et al. (2003) at $z \sim 3$, by Djorgovski and collaborators at $z \gtrsim 4$ (Djorgovski et al. 1999, 2003; Djorgovski 1999; Stiavelli et al. 2005), and by Willott et al. (2005) at $z \sim 6$. The binaries in our sample offer an opportunity to conduct analogous studies over a range of lower and more accessible redshifts, with the added bonus that one expects these extremely rare binary systems to trace even richer environments.

Measurements of the shape of the quasar-quasar and quasar-galaxy correlation function on the small scales probed by our binaries will yield valuable insights into the physical processes that trigger quasar activity and will help explain how quasars are embedded in the structure formation hierarchy. Reproducing the excess clustering with semianalytical models (Kauffmann & Haehnelt 2002) and halo models (see, e.g., PMN04) would provide constraints on the distribution of quasars in dark matter halos. Another interesting question is whether the quasars in these binaries have significantly longer lifetimes than "field" quasars (Haiman & Hui 2001; Martini & Weinberg 2001), which would have interesting implications for the masses of supermassive black holes (Wyithe & Loeb 2005) in the richest regions of the universe.

We close with the reminder that our survey for quasar pairs is ongoing and less than 50% complete. We expect to find a comparable number of binaries in the current SDSS quasar sample. Furthermore, the faint photometric quasar selection techniques of Richards et al. (2004) aim to construct a sample of $\sim 10^6$ quasars. Extrapolating from the number of pairs published here, we would expect to find ~ 1000 new binaries in a sample of this size, which would allow a much more precise measurement of the correlation function on small scales.

J. F. H. wishes to thank his thesis advisor David Spergel for advice, guidance, and helpful discussions over the course of this work during his time in Princeton. For part of this study, J. F. H. was supported by the Proctor Graduate Fellowship at Princeton University and by a generous gift from the Paul and Daisy Soros Fellowship for New Americans. The program is not responsible for the views expressed. J. F. H. is currently supported by NASA through Hubble Fellowship grant 01172.01-A awarded by the Space Telescope Science Institute, which is operated by the Association of Universities for Research in Astronomy, Inc., for NASA, under contract NAS5-26555. Thanks to Bob Nichol and Alex Gray for help with the faint photometric quasar catalog. We are grateful to the observing specialists at Apache Point Observatory, Russet MacMillan, John Barentine, Bill Ketzeback, and

Jack Dembicky, for many nights of hard work. D. P. S. acknowledges support from NSF grant AST 03-07582, and M. A. S. acknowledges the support of NSF grant AST 03-07409. Finally, we wish to thank the anonymous referee for constructive comments.

Funding for the creation and distribution of the SDSS Archive has been provided by the Alfred P. Sloan Foundation, the Participating Institutions, the National Aeronautics and Space Administration, the National Science Foundation, the US Department of Energy, the Japanese Monbukagakusho, and the Max Planck Society. The SDSS Web site is at http://www.sdss.org. The SDSS is managed by the Astrophysical Research Consortium for the Participating Institutions. The Participating Institutions are the University of Chicago, Fermilab, the Institute for Advanced Study, the Japan Participation Group, The Johns Hopkins University, the Korean Scientist Group, Los Alamos National Laboratory, the Max Planck Institute for Astronomy, the Max Planck Institute for Astrophysics, New Mexico State University, the University of Pittsburgh, the University of Portsmouth, Princeton University, the United States Naval Observatory, and the University of Washington.

This paper is based in part on data collected at the W. M. Keck Observatory, the Apache Point Observatory 3.5 m telescope, the Hobby-Eberly Telescope, and the European Southern Observatory, Chile (proposal 67.A-0544). The Apache Point Observatory 3.5 m telescope is owned and operated by the Astrophysical Research Consortium. The W. M. Keck Observatory is operated as a scientific partnership among the California Institute of Technology, the University of California, and NASA. The Hobby-Eberly Telescope is a joint project of the University of Texas at Austin, the Pennsylvania State University, Stanford University, Ludwig-Maximillians-Universität München, and Georg-August-Universität Göttingen. The Hobby-Eberly Telescope is named in honor of its principal benefactors, William P. Hobby and Robert E. Eberly. The Marcario Low-Resolution Spectrograph is named for Mike Marcario of High Lonesome Optics, who fabricated several optics for the instrument but died before its completion; it is a joint project of the Hobby-Eberly Telescope partnership and the Instituto de Astronomía de la Universidad Nacional Autónoma de México.

APPENDIX

In this appendix we present the results of all our follow-up observations not included above, as well as the list of projected pairs of quasars in the SDSS quasar sample that have similar redshifts. These tables will facilitate future studies of close quasar pairs and prevent the duplicate observations of candidates already observed by the SDSS or our follow-up observation program.

In Table 8 we list all projected pairs of quasars in the combined SDSS + 2QZ spectroscopic catalog with angular separations $\theta < 90''$ and redshift difference $\Delta z < 0.5$. All projected pairs of quasars discovered from our follow-up spectroscopic observations are listed in Table 9. Finally, Table 10 lists all the quasar-star pairs identified from our follow-up observations. The full versions of these tables are published in the electronic version of this article.

TABLE 8

PROJECTED PAIRS OF QUASARS DISCOVERED IN OVERLAPPING PLATES

Name	R.A. (J2000.0)	Decl. (J2000.0)	u	g	r	i	z	z	$\Delta\theta$	$R_{\rm prop}$
SDSS J0005+0102A	00 05 00.84	+01 03 03.3	19.50	19.26	19.20	18.93	18.81	1.63	42.7	259.7
SDSS J0005+0102B	00 05 00.54	+01 02 20.8	18.67	18.45	18.33	18.27	18.10	2.12		
SDSS J0008−0039A	00 08 04.23	−00 39 23.0	20.79	20.41	20.25	19.97	19.72	1.61	27.7	168.6
SDSS J0008−0039B	00 08 05.18	−00 39 46.8	20.53	20.53	20.56	20.16	20.11	1.94		

NOTES.—Units of right ascension are hours, minutes, and seconds, and units of declination are degrees, arcminutes, and arcseconds. Quasars labeled "SDSS" or "2QZ" are members of the SDSS or 2QZ spectroscopic quasar catalog. The redshift of each quasar is indicated by the second "z" column, and the foreground quasar is always designated "A." The column labeled $R_{\rm prop}$ is the transverse proper separation (in h^{-1} kpc), evaluated at the foreground quasar redshift, and $\Delta\theta$ is the angular separation in arcseconds. Extinction-corrected SDSS five-band PSF photometry is given in the columns u, g, r, i, and z. Table 8 is published in its entirety in the electronic edition of the *Astronomical Journal*. A portion is shown here for guidance regarding its form and content.

TABLE 9

PROJECTED PAIRS OF QUASARS DISCOVERED FROM FOLLOW-UP SPECTROSCOPY

Name	R.A. (J2000.0)	Decl. (J2000.0)	u	g	r	i	z	z	$\Delta\theta$	R	χ^2
SDSS J0002−0053A	00 02 12.53	−00 53 11.7	20.72	20.59	20.34	20.12	20.17	1.54	7.3	44.5	20.9
SDSS J0002−0053B	00 02 12.53	−00 53 11.7	20.10	19.64	19.52	19.41	19.23	2.21			
SDSS J0036−1109A	00 36 49.63	−11 09 29.8	19.08	18.85	18.67	18.45	18.67	1.51	4.7	28.5	19.0
SDSS J0036−1109B	00 36 49.63	−11 09 29.8	20.92	20.64	20.46	20.52	20.24	2.18			

NOTES.—Units of right ascension are hours, minutes, and seconds, and units of declination are degrees, arcminutes, and arcseconds. Quasars labeled "A" are members of the SDSS or 2QZ spectroscopic quasar catalogs. Quasars discovered from follow-up spectroscopy are designated by "B." For projected pairs discovered from the photometric catalog, "A" designates the brighter of the two quasars. The redshift of each quasar is indicated by the second "z" column. The column labeled $R_{\rm prop}$ is the transverse proper separation (in h^{-1} kpc), evaluated at the foreground quasar redshift, and $\Delta\theta$ is the angular separation in arcseconds. Extinction-corrected SDSS five-band PSF photometry is given in the columns u, g, r, i, and z, and χ^2 is the value of our color similarity statistic. Table 9 is published in its entirety in the electronic edition of the *Astronomical Journal*. A portion is shown here for guidance regarding its form and content.

TABLE 10

QUASAR-STAR PAIRS DISCOVERED FROM FOLLOW-UP SPECTROSCOPY

Name	R.A. (J2000.0)	Decl. (J2000.0)	u	g	r	i	z	z	$\Delta\theta$	χ^2
SDSS J0006+0026A	00 06 14.00	+00 26 05.0	20.85	20.09	19.98	19.95	19.81	2.51	28.0	42.4
SDSS J0006+0026B	00 06 14.00	+00 26 05.0	21.04	20.16	19.83	19.70	19.78			
SDSS J0015+0048A	00 15 57.08	+00 48 22.4	20.74	19.95	19.63	19.57	19.29	2.31	53.5	5.4
SDSS J0015+0048B	00 15 57.08	+00 48 22.4	21.12	20.38	20.08	19.96	19.87			

NOTES.—Units of right ascension are hours, minutes, and seconds, and units of declination are degrees, arcminutes, and arcseconds. Quasars labeled "A" are members of the SDSS or 2QZ spectroscopic quasar catalog. Stars discovered from follow-up spectroscopy are designated by "B." The redshift of the quasar is indicated by the second "z" column, extinction-corrected SDSS five-band PSF photometry is given in the columns u, g, r, i, and z, $\Delta\theta$ is the angular separation in arcseconds, and χ^2 is the value of our color similarity statistic. Table 10 is published in its entirety in the electronic edition of the *Astronomical Journal*. A portion is shown here for guidance regarding its form and content.

REFERENCES

Abazajian, K., et al. 2003, AJ, 126, 2081
———. 2004, AJ, 128, 502
———. 2005, AJ, 129, 1755
Adelberger, K. L., & Steidel, C. C. 2005, ApJ, 630, 50
Adelberger, K. L., Steidel, C. C., Shapley, A. E., & Pettini, M. 2003, ApJ, 584, 45
Anderson, S. F., et al. 2003, AJ, 126, 2209
Andreani, P., & Cristiani, S. 1992, ApJ, 398, L13
Bahcall, J. N., Kirhakos, S., Saxe, D. H., & Schneider, D. P. 1997, ApJ, 479, 642
Bahcall, J. N., Schmidt, M., & Gunn, J. E. 1969, ApJ, 157, L77
Bahcall, N. A., & Chokshi, A. 1991, ApJ, 380, L9
Barnes, J. E., & Hernquist, L. 1996, ApJ, 471, 115
Becker, R. H., White, R. L., & Helfand, D. J. 1995, ApJ, 450, 559
Blanton, M. R., Lin, H., Lupton, R. H., Maley, F. M., Young, N., Zehavi, I., & Loveday, J. 2003, AJ, 125, 2276
Bonnet, H., Fort, B., Kneib, J.-P., Mellier, Y., & Soucail, G. 1993, A&A, 280, L7
Boyle, B. J., Shanks, T., Croom, S. M., Smith, R. J., Miller, L., Loaring, N., & Heymans, C. 2000, MNRAS, 317, 1014
Brown, M. J. I., Boyle, B. J., & Webster, R. L. 2001, AJ, 122, 26
Budavári, T., et al. 2001, AJ, 122, 1163
Carlberg, R. G. 1990, ApJ, 350, 505
Castander, F. J., et al. 2001, AJ, 121, 2331
Coil, A. L., et al. 2004, ApJ, 609, 525
Cole, S., & Kaiser, N. 1989, MNRAS, 237, 1127
Crampton, D., Cowley, A. P., Hickson, P., Kindl, E., Wagner, R. M., Tyson, J. A., & Gullixson, C. 1988, ApJ, 330, 184
Croom, S. M., Boyle, B. J., Loaring, N. S., Miller, L., Outram, P. J., Shanks, T., & Smith, R. J. 2002, MNRAS, 335, 459
Croom, S. M., & Shanks, T. 1996, MNRAS, 281, 893
Croom, S. M., Shanks, T., Boyle, B. J., Smith, R. J., Miller, L., Loaring, N. S., & Hoyle, F. 2001, MNRAS, 325, 483
Croom, S. M., Smith, R. J., Boyle, B. J., Shanks, T., Miller, L., Outram, P. J., & Loaring, N. S. 2004a, MNRAS, 349, 1397
Croom, S., et al. 2004b, in ASP Conf. Ser. 311, AGN Physics with the Sloan Digital Sky Survey, ed. G. T. Richards & P. B. Hall (San Francisco: ASP), 457
———. 2005, MNRAS, 356, 415
Djorgovski, S. 1991, in ASP Conf. Ser. 21, The Space Distribution of Quasars, ed. D. Crampton (San Francisco: ASP), 349
Djorgovski, S. G. 1999, in ASP Conf. Ser. 193, The Hy-Redshift Universe: Galaxy Formation and Evolution at High Redshift, ed. A. J. Bunker & W. J. M. van Breugel (San Francisco: ASP), 397
Djorgovski, S. G., Odewahn, S. C., Gal, R. R., Brunner, R. J., & de Carvalho, R. R. 1999, in ASP Conf. Ser. 191, Photometric Redshifts and High-Redshift Galaxies, ed. R. J. Weymann et al. (San Francisco: ASP), 179
Djorgovski, S. G., Stern, D., Mahabal, A. A., & Brunner, R. 2003, ApJ, 596, 67
Duncan, R. C. 1991, ApJ, 375, L41
Efstathiou, G., & Rees, M. J. 1988, MNRAS, 230, 5P
Eisenstein, D. J., et al. 2001, AJ, 122, 2267
Ellingson, E., Yee, H. K. C., & Green, R. F. 1991, ApJ, 371, 49
Epps, H. W., & Miller, J. S. 1998, Proc. SPIE, 3355, 48
Fan, X., et al. 1999, AJ, 118, 1
———. 2001, AJ, 121, 54
Ferrarese, L., & Merritt, D. 2000, ApJ, 539, L9
Finn, R. A., Impey, C. D., & Hooper, E. J. 2001, ApJ, 557, 578
Fischer, P., Tyson, J. A., Bernstein, G. M., & Guhathakurta, P. 1994, ApJ, 431, L71
Fisher, K. B., Bahcall, J. N., Kirhakos, S., & Schneider, D. P. 1996, ApJ, 468, 469
Fukugita, M., Ichikawa, T., Gunn, J. E., Doi, M., Shimasaku, K., & Schneider, D. P. 1996, AJ, 111, 1748
Fukugita, M., Nakamura, O., Schneider, D. P., Doi, M., & Kashikawa, N. 2004, ApJ, 603, L65
Gebhardt, K., et al. 2000, ApJ, 539, L13
Gehrels, N. 1986, ApJ, 303, 336
Green, P. J., et al. 2002, ApJ, 571, 721
Gregg, M. D., Becker, R. H., White, R. L., Richards, G. T., Chaffee, F. H., & Fan, X. 2002, ApJ, 573, L85
Gunn, J. E., et al. 1998, AJ, 116, 3040
Guzik, J., & Seljak, U. 2002, MNRAS, 335, 311
Haehnelt, M. G., & Rees, M. J. 1993, MNRAS, 263, 168
Hagen, H.-J., Hopp, U., Engels, D., & Reimers, D. 1996, A&A, 308, L25
Haiman, Z., & Hui, L. 2001, ApJ, 547, 27
Hall, P. B., & Green, R. F. 1998, ApJ, 507, 558
Hall, P. B., Green, R. F., & Cohen, M. 1998, ApJS, 119, 1
Hawkins, M. R. S., Clements, D., Fried, J. W., Heavens, A. F., Véron, P., Minty, E. M., & van der Werf, P. 1997, MNRAS, 291, 811
Hennawi, J. F. 2005, Ph.D. thesis, Princeton Univ.
Hennawi, J. F., Dalal, N., & Bode, P. 2005, ApJ, submitted (astro-ph/0506175)
Hewett, P. C., Foltz, C. B., Harding, M. E., & Lewis, G. F. 1998, AJ, 115, 383
Hewett, P. C., Webster, R. L., Harding, M. E., Jedrzejewski, R. J., Foltz, C. B., Chaffee, F. H., Irwin, M. J., & Le Fevre, O. 1989, ApJ, 346, L61
Hogan, C., & Narayan, R. 1984, MNRAS, 211, 575
Hogg, D. W., Baldry, I. K., Blanton, M. R., & Eisenstein, D. J. 2002, preprint (astro-ph/0210394)
Hogg, D. W., Finkbeiner, D. P., Schlegel, D. J., & Gunn, J. E. 2001, AJ, 122, 2129
Hopkins, P. F., et al. 2004, AJ, 128, 1112
Inada, N., et al. 2003a, AJ, 126, 666
———. 2003b, Nature, 426, 810
Infante, L., Varela, J., Moles, M., Hertling, G., García, A., & Menanteau, F. 2003, ApJ, 588, 90
Iovino, A., & Shaver, P. A. 1988, ApJ, 330, L13
Kaiser, N. 1984, ApJ, 284, L9
Kauffmann, G., & Haehnelt, M. G. 2002, MNRAS, 332, 529
Kochanek, C. S., Falco, E. E., & Muñoz, J. A. 1999, ApJ, 510, 590
Koopmans, L. V. E., et al. 2000, A&A, 361, 815
Kruszewski, A. 1988, Acta Astron., 38, 155
Kundic, T. 1997, ApJ, 482, 631
Lacey, C., & Cole, S. 1993, MNRAS, 262, 627
La Franca, F., Andreani, P., & Cristiani, S. 1998, ApJ, 497, 529
Laurikainen, E., & Salo, H. 1995, A&A, 293, 683
Lidz, A., Hui, L., Crotts, A. P. S., & Zaldarriaga, M. 2003, ApJ, submitted (astro-ph/0309204)
Lupton, R. H., Gunn, J. E., Ivezić, Z., Knapp, G. R., Kent, S., & Yasuda, N. 2001, in ASP Conf. Ser. 238, Astronomical Data Analysis Software and Systems X, ed. F. R. Harnden, Jr., F. A. Primini, & H. E. Payne (San Francisco: ASP), 269
Lupton, R. H., Gunn, J. E., & Szalay, A. S. 1999, AJ, 118, 1406
Magorrian, J., et al. 1998, AJ, 115, 2285
Malhotra, S., Rhoads, J. E., & Turner, E. L. 1997, MNRAS, 288, 138
Martini, P., & Weinberg, D. H. 2001, ApJ, 547, 12
Masjedi, M., et al. 2005, ApJ, submitted
McLure, R. J., & Dunlop, J. S. 2001, MNRAS, 321, 515
Meylan, G., & Djorgovski, S. 1989, ApJ, 338, L1
Miller, L., Lopes, A. M., Smith, R. J., Croom, S. M., Boyle, B. J., Shanks, T., & Outram, P. 2004, MNRAS, 348, 395
Mo, H. J., & Fang, L. Z. 1993, ApJ, 410, 493
Mortlock, D. J., Webster, R. L., & Francis, P. J. 1999, MNRAS, 309, 836
Nusser, A., & Silk, J. 1993, ApJ, 411, L1
Oguri, M., & Keeton, C. R. 2004, ApJ, 610, 663

Oguri, M., et al. 2004, ApJ, 605, 78
———. 2005, ApJ, 622, 106
Oke, J. B., & Gunn, J. E. 1983, ApJ, 266, 713
Oke, J. B., et al. 1995, PASP, 107, 375
Osmer, P. S. 1981, ApJ, 247, 762
Paczyński, B. 1986, Nature, 319, 567
Pello, R., Miralles, J. M., Le Borgne, J.-F., Picat, J.-P., Soucail, G., & Bruzual, G. 1996, A&A, 314, 73
Peng, C. Y., et al. 1999, ApJ, 524, 572
Phinney, E. S., & Blandford, R. D. 1986, Nature, 321, 569
Pier, J. R., Munn, J. A., Hindsley, R. B., Hennessy, G. S., Kent, S. M., Lupton, R. H., & Ivezić, Ž. 2003, AJ, 125, 1559
Pindor, B., Turner, E. L., Lupton, R. H., & Brinkmann, J. 2003, AJ, 125, 2325
Pindor, B., et al. 2006, AJ, 131, 41
Porciani, C., Magliocchetti, M., & Norberg, P. 2004, MNRAS, 355, 1010 (PMN04)
Richards, G. T., Vanden Berk, D. E., Reichard, T. A., Hall, P. B., Schneider, D. P., SubbaRao, M., Thakar, A. R., & York, D. G. 2002a, AJ, 124, 1
Richards, G. T., et al. 2001a, AJ, 121, 2308
———. 2001b, AJ, 122, 1151
———. 2002b, AJ, 123, 2945
———. 2003, AJ, 126, 1131
———. 2004, ApJS, 155, 257
———. 2005, MNRAS, 360, 839
Schlegel, D. J., Finkbeiner, D. P., & Davis, M. 1998, ApJ, 500, 525
Schneider, D. P., Schmidt, M., & Gunn, J. E. 1994, AJ, 107, 1245
Schneider, D. P., et al. 2000, AJ, 120, 2183
———. 2005, AJ, 130, 367
Schneider, P. 1993, in Gravitational Lenses in the Universe, ed. J. Surdej et al. (Liège: Univ. Liège), 41
Serber, W., et al. 2005, ApJ, submitted
Shanks, T., & Boyle, B. J. 1994, MNRAS, 271, 753
Shaver, P. A. 1984, A&A, 136, L9
Sheldon, E. S., et al. 2004, AJ, 127, 2544
Small, T. A., & Blandford, R. D. 1992, MNRAS, 259, 725
Small, T. A., Sargent, W. L. W., & Steidel, C. C. 1997, AJ, 114, 2254
Smith, J. A., et al. 2002, AJ, 123, 2121
Smith, R. J., Boyle, B. J., & Maddox, S. J. 1995, MNRAS, 277, 270
———. 2000, MNRAS, 313, 252
Spergel, D. N., et al. 2003, ApJS, 148, 175
Sramek, R. A., & Weedman, D. W. 1978, ApJ, 221, 468
Steidel, C. C., Adelberger, K. L., Shapley, A. E., Pettini, M., Dickinson, M., & Giavalisco, M. 2003, ApJ, 592, 728
Steidel, C. C., & Sargent, W. L. W. 1991, AJ, 102, 1610
Stephens, A. W., Schneider, D. P., Schmidt, M., Gunn, J. E., & Weinberg, D. H. 1997, AJ, 114, 41
Stiavelli, M., et al. 2005, ApJ, 622, L1
Stoughton, C., et al. 2002, AJ, 123, 485
Strauss, M. A., et al. 2002, AJ, 124, 1810
Subramanian, K., Rees, M. J., & Chitre, S. M. 1987, MNRAS, 224, 283
Toomre, A., & Toomre, J. 1972, ApJ, 178, 623
Tremaine, S., et al. 2002, ApJ, 574, 740
Turner, E. L. 1991, AJ, 101, 5
Turner, E. L., Goldberg, R. E., & Gunn, J. E. 1982, BAAS, 14, 974
Vanden Berk, D. E., et al. 2001, AJ, 122, 549
———. 2005, AJ, 129, 2047
Vilenkin, A. 1984, ApJ, 282, L51
Wake, D. A., et al. 2004, ApJ, 610, L85
Walsh, D., Carswell, R. F., & Weymann, R. J. 1979, Nature, 279, 381
Weedman, D. W., Weymann, R. J., Green, R. F., & Heckman, T. M. 1982, ApJ, 255, L5
Weinstein, M. A., et al. 2004, ApJS, 155, 243
Willott, C. J., Percival, W. J., McLure, R. J., Crampton, D., Hutchings, J. B., Jarvis, M. J., Sawicki, M., & Simard, L. 2005, ApJ, 626, 657
Wold, M., Lacy, M., Lilje, P. B., & Serjeant, S. 2001, MNRAS, 323, 231
Wyithe, J. S. B., & Loeb, A. 2002a, ApJ, 577, 57
———. 2002b, ApJ, 581, 886
———. 2005, ApJ, 621, 95
Yee, H. K. C., & Green, R. F. 1984, ApJ, 280, 79
———. 1987, ApJ, 319, 28
York, D. G., et al. 2000, AJ, 120, 1579
Yu, Q., & Tremaine, S. 2002, MNRAS, 335, 965
Zehavi, I., et al. 2004, ApJ, 608, 16